Exploring Metal Carbamates as Precursors for the Synthesis of Metal-Organic Frameworks

Stefania Volante,[a,b] Matous Kloda,[c] Jan Demel,[c] Guido Pampaloni,[a,b] Fabio Marchetti,[a,b] Giulio Bresciani,[a,b*] Marco Taddei.[a,b*]

[a] University of Pisa, Dipartimento di Chimica e Chimica Industriale, 56124 Pisa, Italy.

[b] CIRCC, Via Celso Ulpiani 27, I-70126 Bari, Italy.

[c] Institute of Inorganic Chemistry of the Czech Academy of Sciences, Husinec-Řež-1001, 250 68 Řež, Czech Republic

*E-mail addresses: giulio.bresciani@dcci.unipi.it; marco.taddei@unipi.it

ELECTRONIC SUPPLEMENTARY INFORMATION

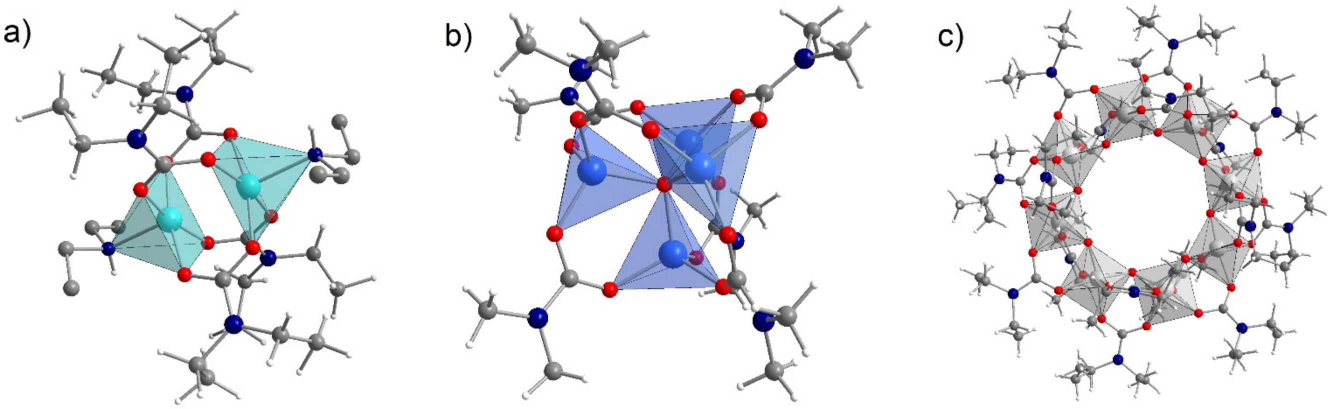

Figure S1: Structures of $Cu_2(O_2CNEt_2)_4{\cdot}(HNEt_2)_2$ (left), $Zn_4O(O_2CNMe_2)_6$ (center) and $Ti_8O_8(O_2CNEt_2)_{16}$ (right). These structures are analogous of SBUs found in HKUST-1, UiO-66 and MIL-125, respectively.

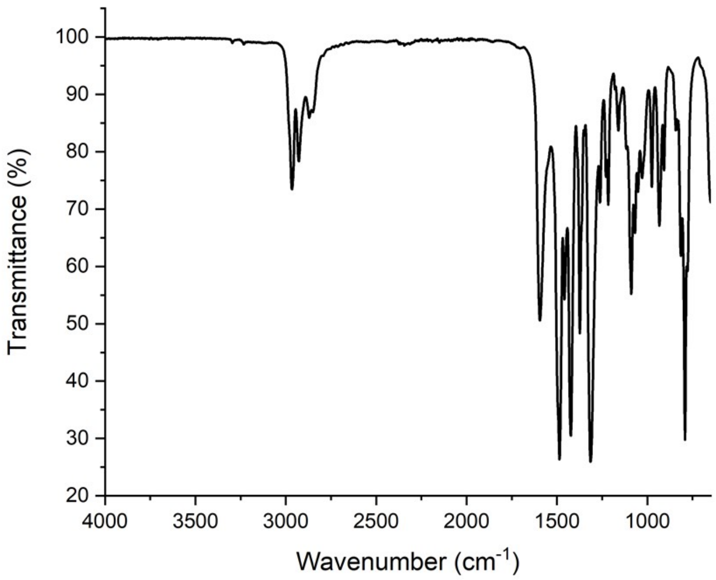

Figure S2: IR spectrum of $Cu_2(O_2CNEt_2)_4 \cdot 2NHEt_2$ (**CuCBM**)

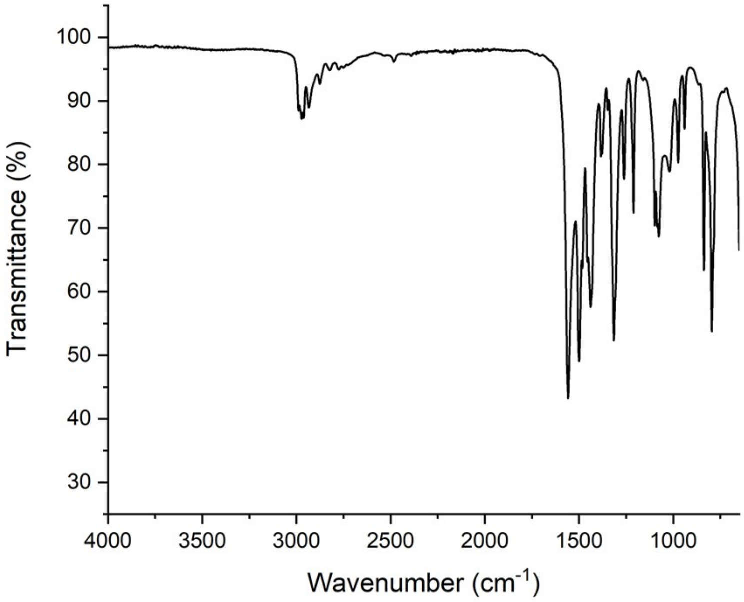

Figure S3: IR spectrum of $Zr(O_2CNEt_2)_4$ (**ZrCBM**).

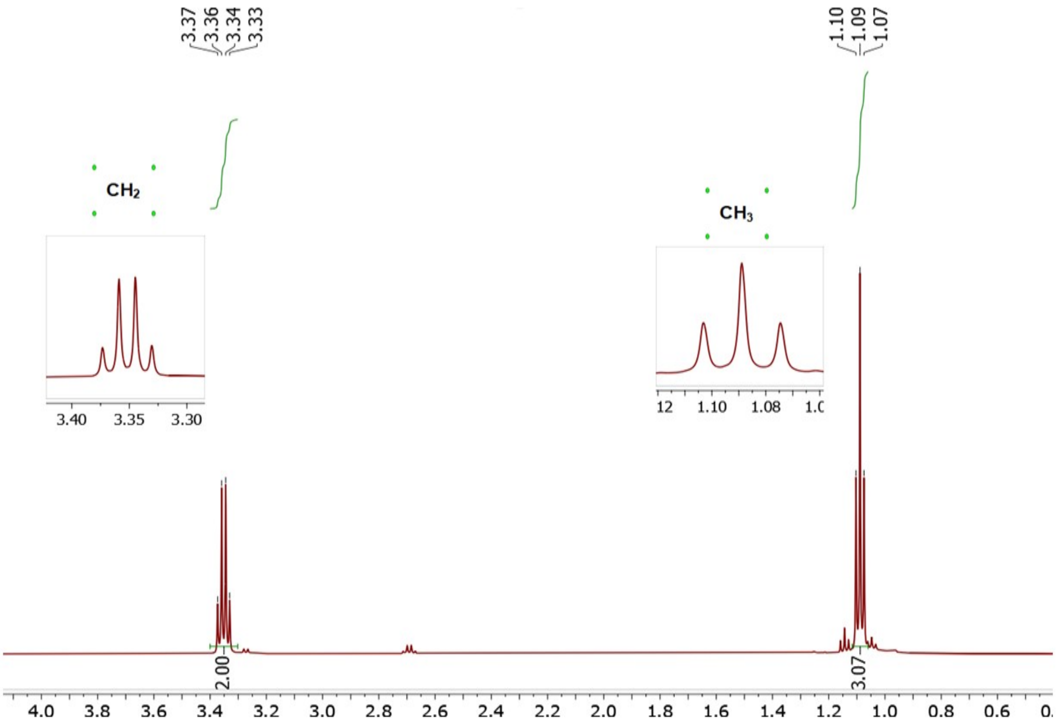

Figure S4: ^{1}H NMR spectrum (400MHz, CDCl$_3$) of Zr(O$_2$CNEt$_2$)$_4$ (**ZrCBM**).

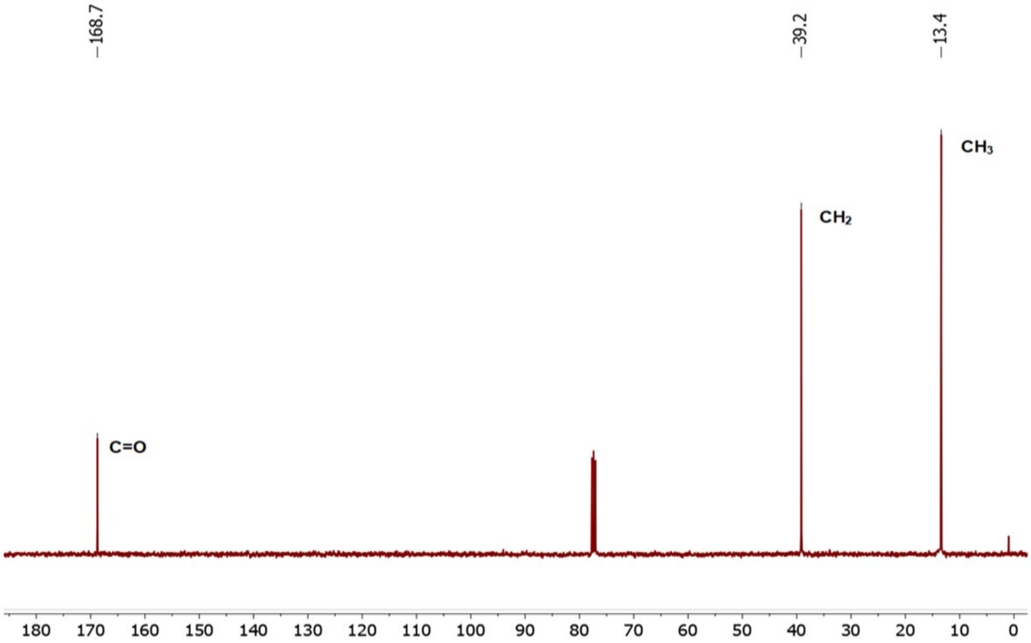

Figure S5: ^{13}C NMR spectrum (100 MHz, CDCl$_3$) of Zr(O$_2$CNEt$_2$)$_4$ (**ZrCBM**).

Table S1: Syntheses of HKUST-1 conducted in DMF. The precursors are: **CuCBM** = Copper (II) *N,N*-diethylcarbamate, **CuOAc** = Copper (II) Acetate, **$CuCl_2$** = Anhydrous copper(II) chloride. The linker is **P** = H_3BTC. The addition methods are **s** = single addition, **g** = gradual addition. FWHM (Full width at half maximum) was evaluated for the 222 reflection located at 11.6 °2θ.

Entry	Sample	Linker Addition method	Yield (mg)	FWHM (°)
1	**CuOAc_DMF-P-T140-s**	Single	94	0.22
2	**CuCBM_DMF-P-T140-s**	Single	96	0.20
3	**$CuCl_2$_DMF-P-T140-s**	Single	No product	---
4	**CuOAc_DMF-P-s**	Single	No product	---
5	**CuCBM_DMF-P-s**	Single	99	0.27
6	**$CuCl_2$_DMF-P-s**	Single	No product	---
7	**CuCBM_DMF-P-g**	Gradual	98	0.23

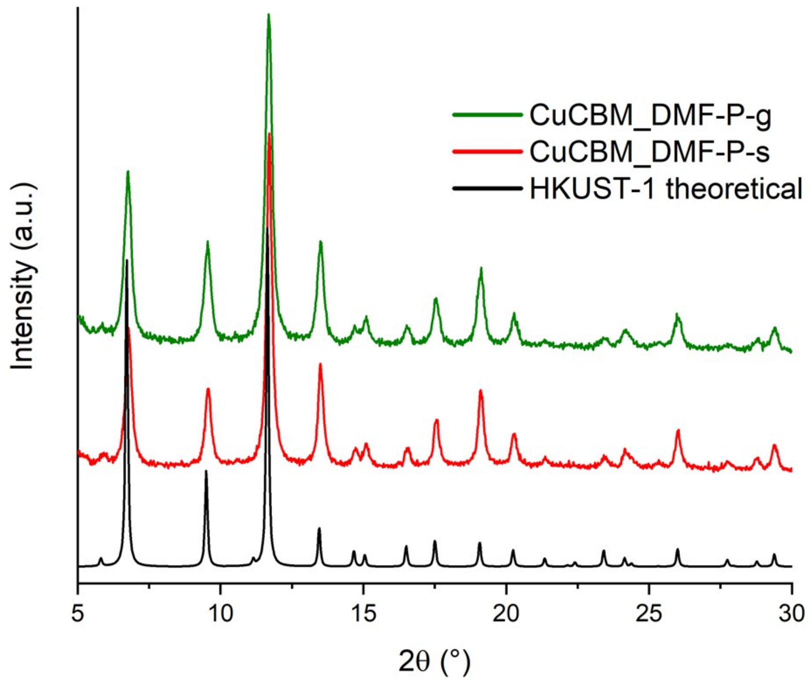

Figure S6: PXRD patterns of **CuCBM_DMF-P-g** (green line), **CuCBM_DMF-P-s** (red line), and the theoretical pattern of HKUST-1 (black line).

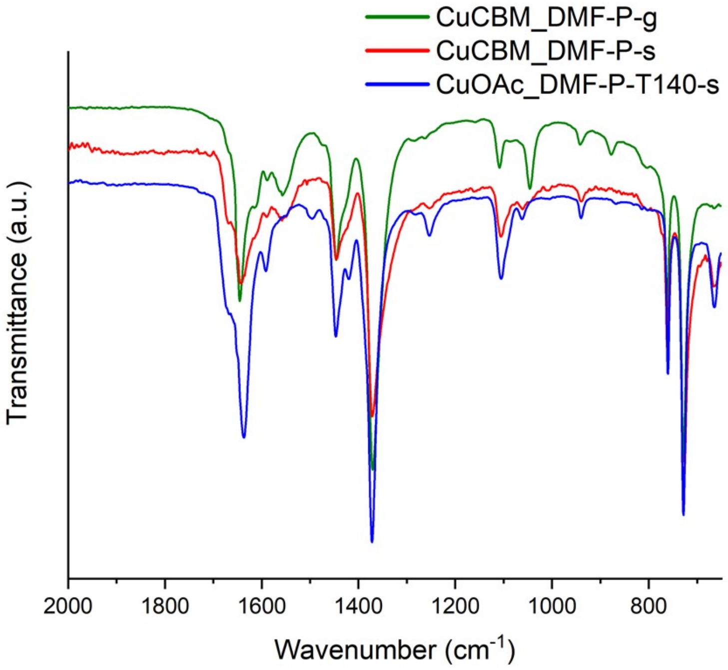

Figure S7: IR spectra of **CuCBM_DMF-P-g** (green line), **CuCBM_DMF-P-s** (red line) and **CuOAc_DMF-P-T140-s** (blue line) used as reference.

Table S2: Syntheses of HKUST-1 conducted in DMF with deprotonated linker. Linkers are **D^{I}** = H_2BTC^{-}, **D^{II}** = $HBTC^{2-}$, **D^{III}** = BTC^{3-}. The addition methods are **s** = single addition, **g** = gradual addition. FWHM (Full width at half maximum) was evaluated for the 222 reflection located at 11.6 °2θ.

Entry	**Sample name**	**Deprotonating agent**	**Linker Addition method**	**Yield (mg)**	**FWHM (°)**
1	**CuOAc_DMF-D^{III}-s**	$NHEt_2$, 3 eq	Single	90	0.28
2	**$CuCl_2$_DMF-D^{III}-s**	$NHEt_2$, 3 eq	Single	103	0.50
3	**CuCBM_DMF-D^{III}-s**	$NHEt_2$, 3 eq	Single	83	0.19
4	**CuCBM_DMF-D^{I}-g**	$NHEt_2$, 1 eq	Gradual	100	0.20
5	**CuCBM_DMF-D^{II}-g**	$NHEt_2$, 2 eq	Gradual	103	0.19
6	**CuCBM_DMF-D^{III}-g**	$NHEt_2$, 3 eq	Gradual	46	0.14

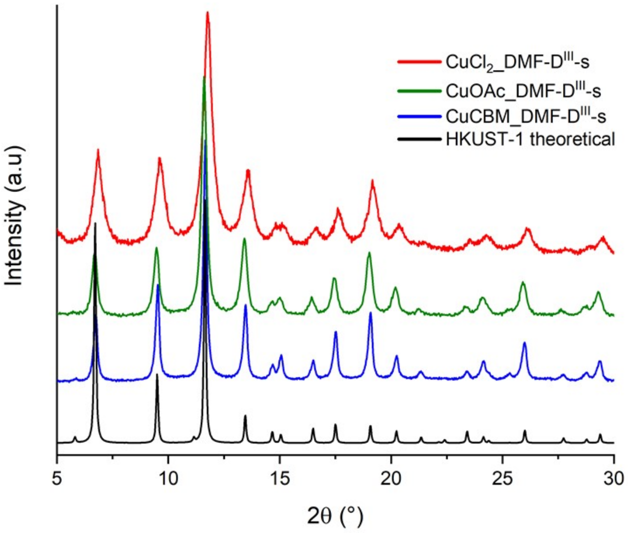

Figure S8: XRD patterns of **$CuCl_2$_DMF-D^{III}-s** (red line), **CuOAc_DMF-D^{III}-s** (green line), **CuCBM_DMF-D^{III}-s** (blue line) compared with the theoretical pattern of HKUST-1 (black line).

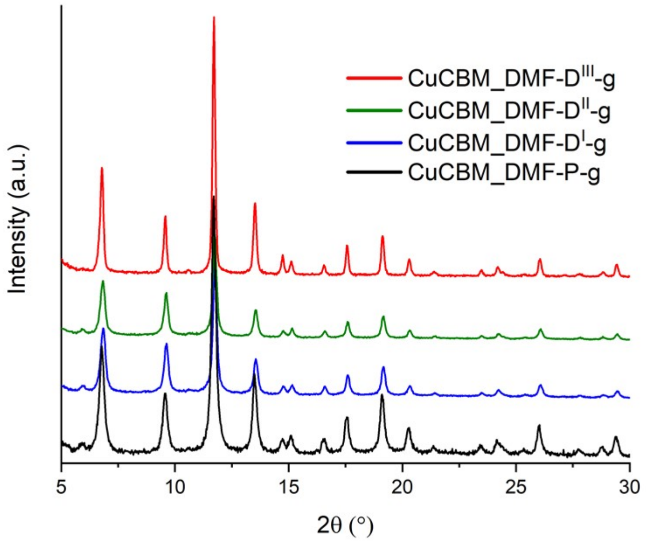

Figure S9: PXRD patterns of **CuCBM_DMF-D^{III}-s** (red line), **CuCBM_DMF-D^{II}-g** (green line), **CuCBM_DMF-D^{I}-g** (blue line) compared with **CuCBM_DMF-P-g** (black line).

Table S3: Syntheses conducted in DMF with deprotonated linker using DBU as the base. The precursors are: **CuCBM** = Copper(II) *N,N*-diethylcarbamate, **CuOAc** = Copper(II) Acetate, **$CuCl_2$** = Anhydrous copper(II) chloride. The linkers are: **D^I** = $H_2BTC^–$, **D^{II}** = $HBTC^{2–}$, **D^{III}** = $BTC^{3–}$. The addition methods is: **s** = single addition. Reaction temperature is 25 °C and reaction time is 24 h. FWHM (Full width at half maximum) was evaluated for the 222 reflection located at 11.6 °2θ.

Entry	Sample name	Deprotonating agent	Linker Addition method	Yield (mg)	FWHM (°)
1	**CuCBM_DMF-D^{III}#-s**	DBU, 3 eq	Single	38	0.57
2	**CuOAc_DMF-D^{III}#-s**	DBU, 3 eq	Single	128	0.59
3	**$CuCl_2$_DMF-D^{III}#-s**	DBU, 3 eq	Single	86	0.44

[**#**] DBU used as deprotonating agent.

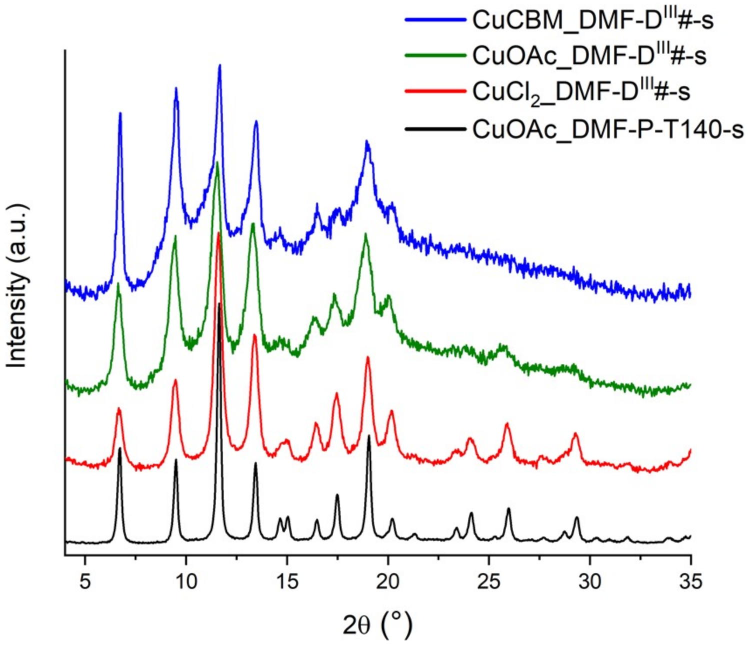

Figure S10: PXRD patterns comparison of **CuCBM_DMF-D^{III}#-s** (blue line), **CuOAc_DMF-D^{III}#-s** (green line), **$CuCl_2$_DMF-D^{III}#-s** (red line) and reference HKUST-1 (black line).

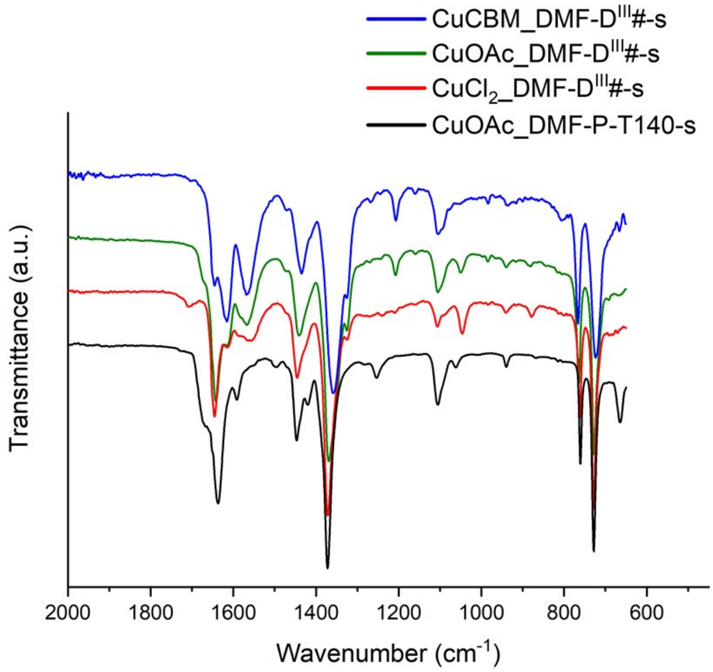

Figure S11: IR spectra of **CuCBM_DMF-D^{III}#-s** (blue line), **CuOAc_DMF-D^{III}#-s** (green line), **CuCl$_2$_DMF-D^{III}#-s** (red line) and reference HKUST-1 (black line). Bands at 1615, 1567 and 1325 cm^{-1} are attributable to DBU.

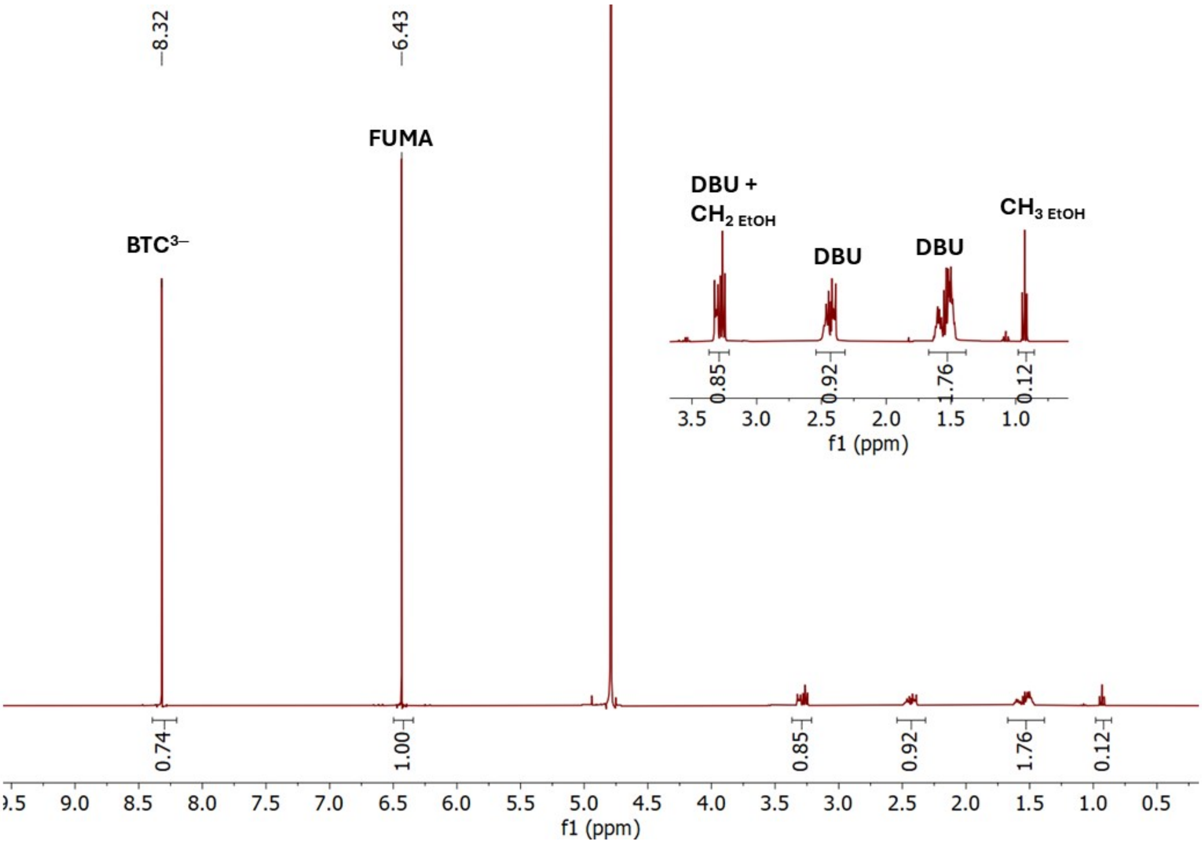

Figure S12: ^{1}H NMR spectrum of **CuCBM_DMF-D^{III}#-s** after digestion, using fumaric acid as internal standard. BTC^{3-} = 1,3,5-benzetricarboxylate anion; FUMA = fumaric acid.

Table S4: Synthesis conducted in conducted in various solvents. The precursor is: **CuCBM** = Copper(II) carbamate. The linkers are: **P** = H_3BTC, **D^I** = H_2BTC^-, **D^{II}** = $HBTC^{2-}$, **D^{III}** = BTC^{3-}. The addition method is: **g** = gradual addition method. Where not specified the reaction temperature is 25 °C, reaction time is 24 h. FWHM (Full width at half maximum) was evaluated for the 222 reflection located at 11.6 °2θ.

Entry	**Sample name**	**Solvent**	**Yield (mg)**	**FWHM (°)**
1	**CuCBM_EtOH-P-g**	EtOH	115	0.26
2	**CuCBM_MeOH-P-g**	MeOH	100	0.27
3	**CuCBM_THF-P-g**	THF	136	---
4	**CuCBM_DIOX-P-g**	1,4-Dioxane	111	0.27
5	**CuOAc_EtOH-P-g**	EtOH	104	---
6	**CuCl2_EtOH-P-g**	EtOH	No product	---
7	**CuCBM_EtOH/H_2O-D^I-g**	EtOH/H_2O	82	0.13
8	**CuCBM_EtOH/H_2O-D^{II}-g**	EtOH/H_2O	82	---
9	**CuCBM_EtOH-D^{III}-g**	EtOH	45	0.26

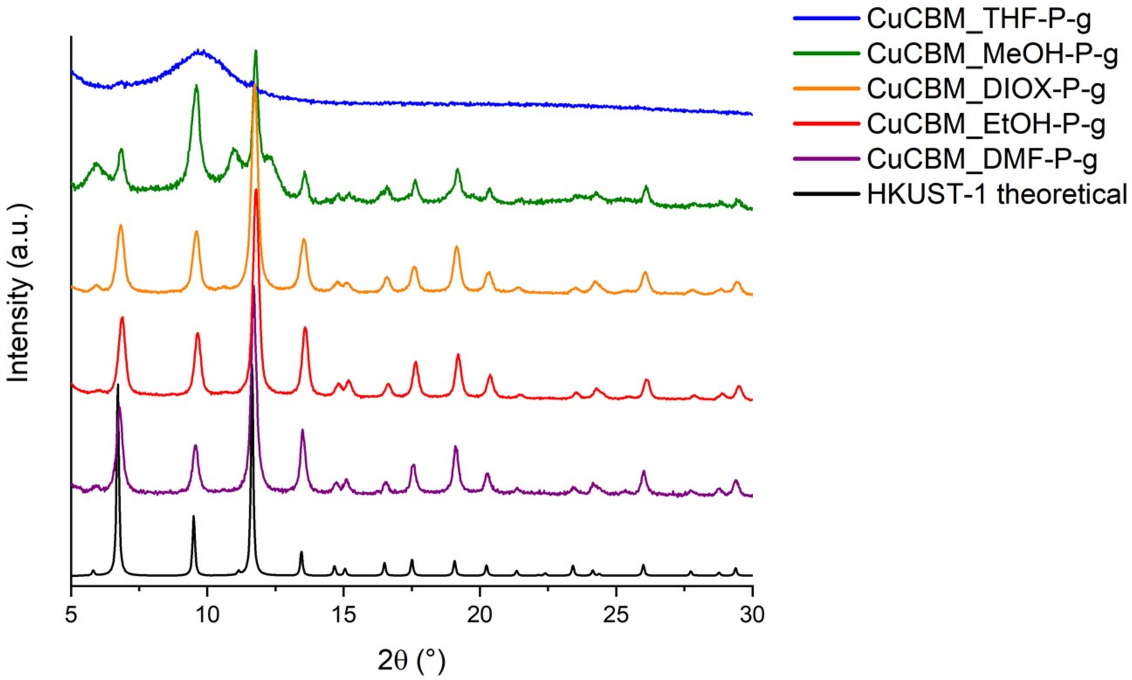

Figure S13: PXRD patterns of **CuCBM_THF-P-g** (blue line), **CuCBM_MeOH-P-g** (green line), **CuCBM_DIOX-P-g** (orange line), **CuCBM_EtOH-P-g** (red line), **CuCBM_DMF-P-g** (purple line) and calculated pattern of HKUST-1 (black line).

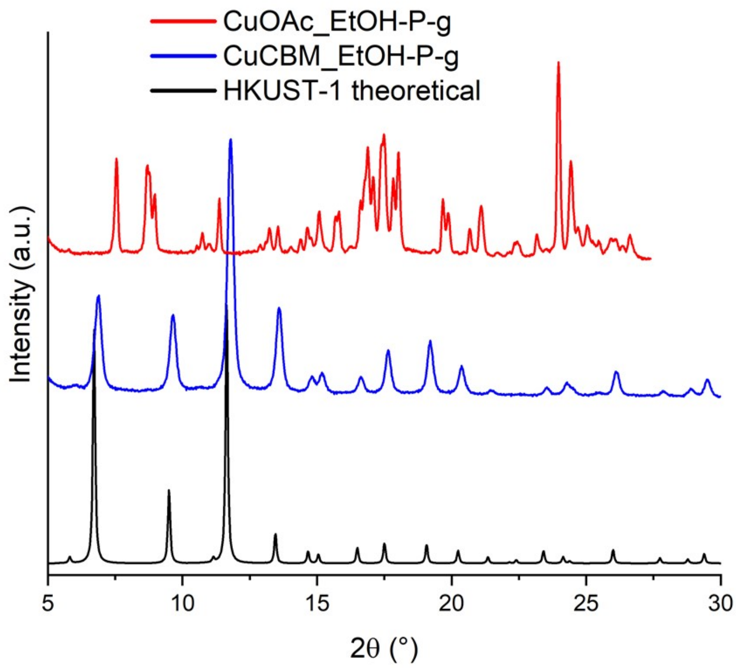

Figure S14: PXRD patterns of **CuOAc_EtOH-P-g** (red line), **CuCBM_EtOH-P-g** (blue line) and theoretical pattern of HKUST-1.

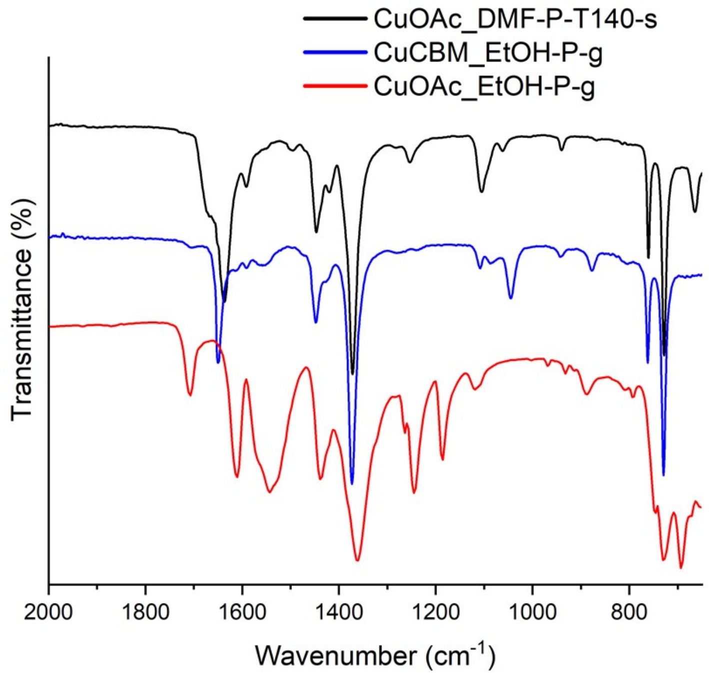

Figure S15: IR spectra of **CuOAc_EtOH-P-g** (red line), **CuCBM_EtOH-P-g** (blue line) and **CuCBM_DMF-P-T140-s** (black line).

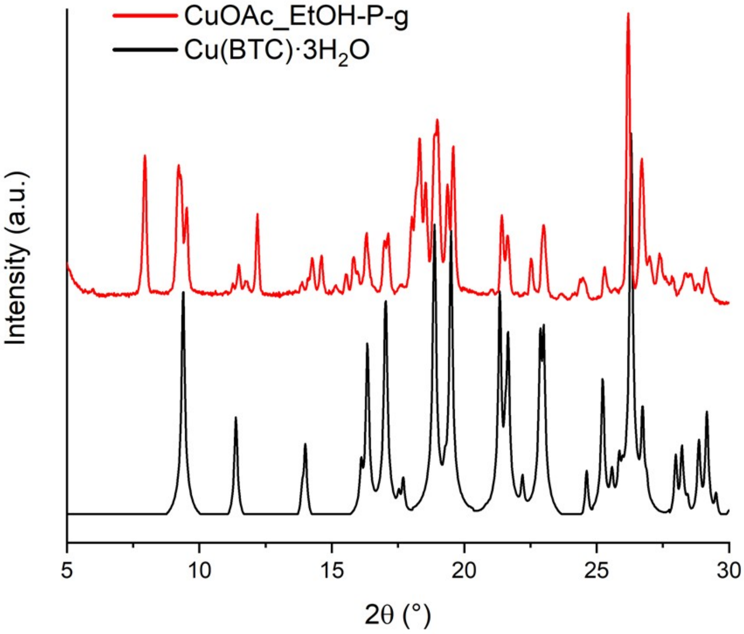

Figure S16: PXRD pattern of **CuOAc_EtOH-P-g** (red line) compared with calculated pattern of $Cu_3(BTC)\cdot3H_2O$ (black line).

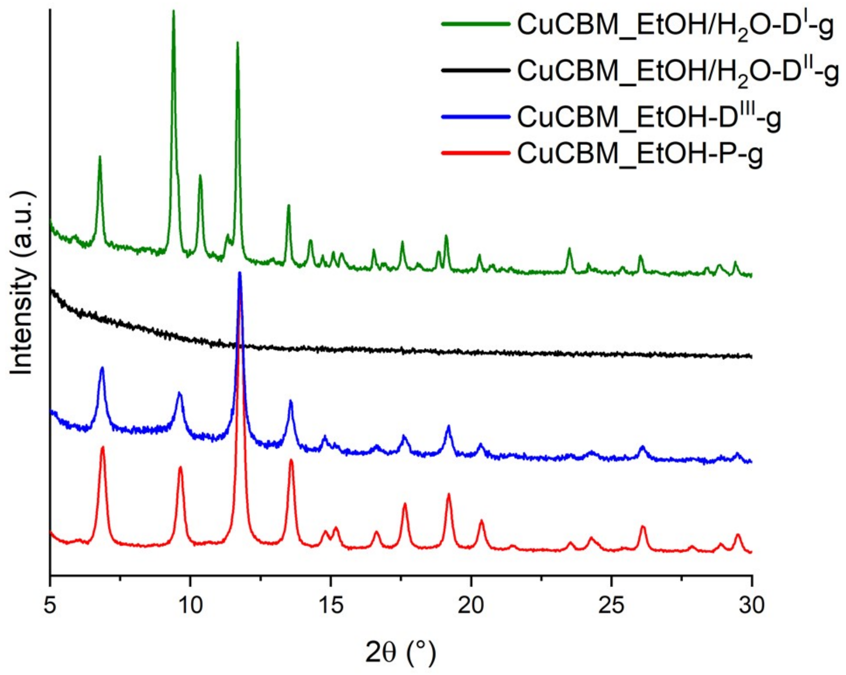

Figure S17: a) PXRD patterns of **CuCBM_EtOH/H_2O-D^I-g** (green line), **CuCBM_EtOH/H_2O-D^{II}-g** (black line), **CuCBM_EtOH-D^{III}-g** (blue line) and **CuCBM_EtOH-P-g** (red line). Given the insolubility of the diethylammonium salts of H_2BTC^- and $HBTC^{2-}$ in pure ethanol, water (8 volume%) was added as a co-solvent for these linkers. The presence of water in the reaction environment led to the formation of either an undesired crystalline impurity when starting from H_2BTC^- or an amorphous product when starting from $HBTC^{2-}$.

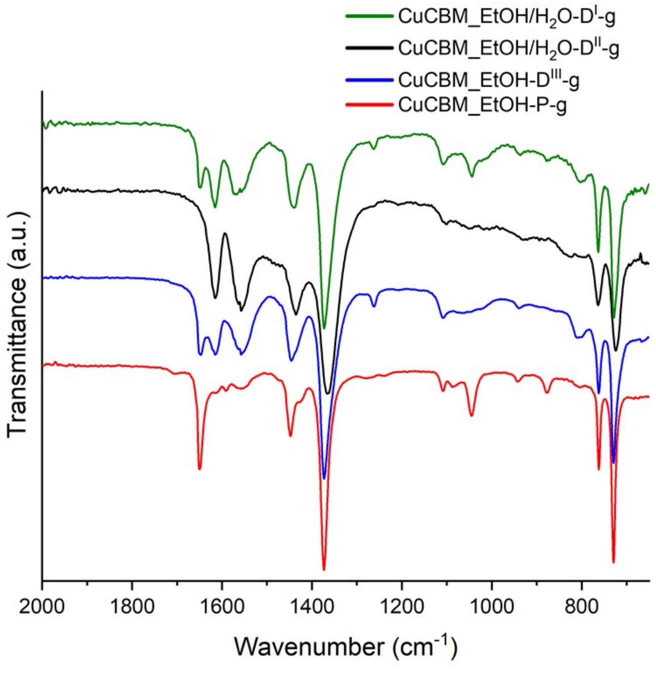

Figure S18: IR spectra of **CuCBM_EtOH/H_2O-D^I-g** (purple line), **CuCBM_EtOH/H_2O -D^{II}-g** (green line), **CuCBM_EtOH-D^{III}-g** (blue line) and **CuCBM_EtOH-P-g** (red line).

Table S5: Syntheses conducted in DMF and EtOH using different addition method. The linker is **P** = H_3BTC. The addition methods are: **g** = gradual addition, **sl** = slow addition using a syringe pump. FWHM (Full width at half maximum) was evaluated for the 222 reflection located at 11.6 °2θ.

Entry	Sample name	Linker Addition method	Yield (mg)	FWHM (°)
1	**CuCBM_DMF-P-g**	Gradual	98	0.23
2	**CuCBM_EtOH-P-g**	Gradual	115	0.26
3	**CuCBM_DMF-P-sl**	Syringe pump	125	0.25
4	**CuCBM_EtOH-P-sl**	Syringe pump	135	0.25

Table S6: One-pot syntheses of HKUST-1. Samples are listed using abbreviations as follows: The precursor is **$CuCl_2$** = Anhydrous copper(II) chloride. The linker is **P** = H_3BTC. The addition methods are **s** = single addition, **sl** = slow addition using a syringe pump. FWHM (Full width at half maximum) was evaluated for the 222 reflection located at 11.6 °2θ.

Entry	Sample name	Solvent	Linker Addition method	Yield (mg)	FWHM
1	**$CuCl_2/NHEt_2/CO_2$_DMF-P-s-3eq**	DMF	Single	109	0.38
2	**$CuCl_2/NHEt_2$_DMF-P-s-3eq**	DMF	Single	67	0.56
3	**$CuCl_2/NHEt_2/CO_2$_DMF-P-s-6eq**	DMF	Single	95	0.35
4	**$CuCl_2/NHEt_2/CO_2$_EtOH-P-s-6eq**	EtOH	Single	78	0.40
5	**$CuCl_2/NHEt_2/CO_2$_DMF-P-sl-6eq**	DMF	Syringe pump	115	0.25
6	**$CuCl_2/NHEt_2/CO_2$_EtOH-P-sl-6eq**	EtOH	Syringe pump	118	0.25

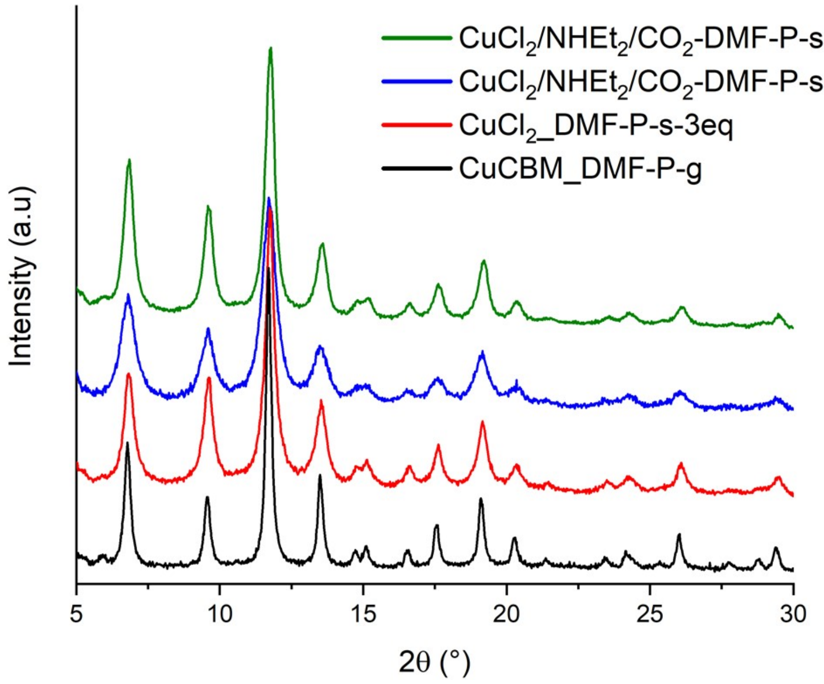

Figure S19: PXRD patterns of **CuCl$_2$/NHEt$_2$/CO$_2$_DMF-P-s-6eq** (green line), **CuCl$_2$/NHEt$_2$/CO$_2$_DMF-P-s-3eq** (blue line), **CuCl$_2$_DMF-P-s-3eq** (red line) and **CuCBM_DMF-P- g** (black line).

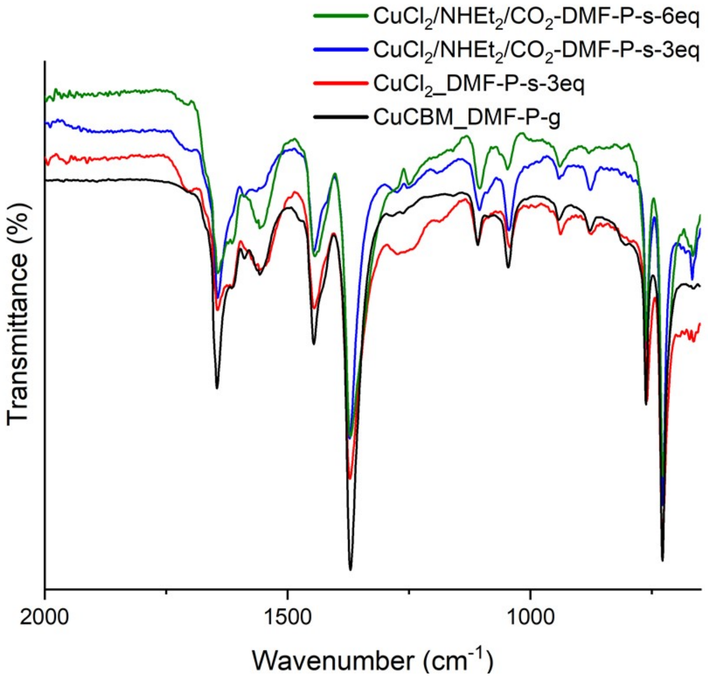

Figure S20: IR spectra of **CuCl$_2$/NHEt$_2$/CO$_2$_DMF-P-s-6eq** (green line), **CuCl$_2$/NHEt$_2$/CO$_2$_DMF-P-s-3eq** (blue line), **CuCl$_2$_DMF-P-s-3eq** (red line) and and **CuCBM_DMF-P- g** (black line).

Scheme S1: A) Carbonation equilibrium of diethylamine to diethylammonium diethylcarbamate. B) Formation of **CuCBM** starting from **$CuCl_2$**. This reaction, when conducted in DMF, is assumed to be an equilibrium. The stoichiometry of this reaction requires at least five equivalents of amine to obtain one equivalent of **CuCBM**.

A)

$$2\ NHEt_2 + CO_2 \rightleftharpoons [NH_2Et_2][O_2CNEt_2]$$

B)

$$CuCl_2 + 2.5\ [NH_2Et_2][O_2CNEt_2] \xrightleftharpoons[+\,CO_2]{-\,CO_2} Cu(O_2CNEt_2)_2 \cdot NHEt_2 + 2\ [NH_2Et_2]Cl$$

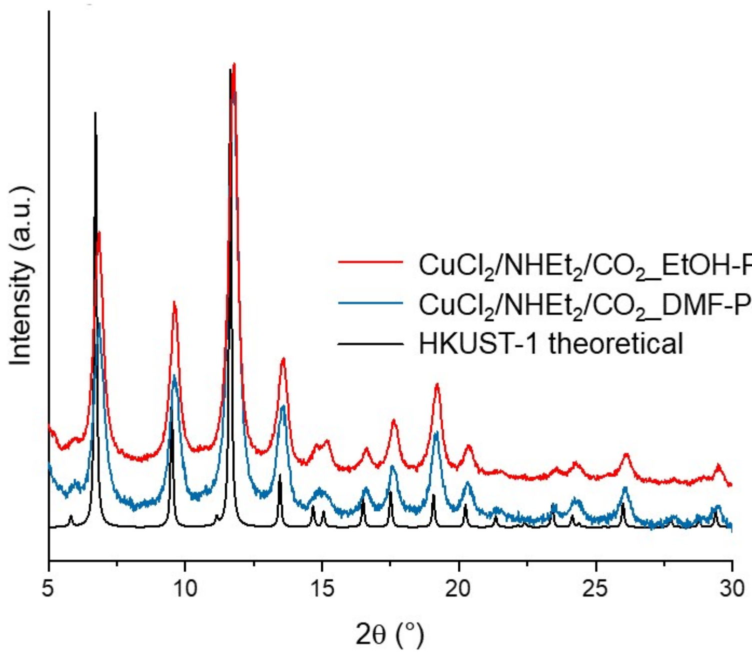

Figure S21: PXRD patterns of **$CuCl_2$/$NHEt_2$/CO_2_EtOH-P-s-6eq** (red line), **$CuCl_2$/$NHEt_2$/CO_2_DMF-P-s-6eq** (blue line) and theoretical pattern of HKUST-1. (black line).

Table S7: Theoretical and experimental percentage of BTC^{3-} ligand for HKUST-1 samples calculated from ^1H-NMR spectra.

Sample	Hypothetical Formula	BTC^{3-} theo [%]	BTC^{3-} exp [%]
CuOAc_DMF-P-T140-s	$Cu_3(BTC)_2(DMF)_{3.30}$	48.9	53.8
CuCBM_DMF-P-sl	$Cu_3(BTC)_2(NHEt_2)_{0.22}(EtOH)_{0.44}$	64.6	64.7
CuCBM_EtOH-P-sl	$Cu_3(BTC)_2(NHEt_2)_{0.40}(EtOH)_{0.60}$	62.6	65.9
$CuCl_2/NHEt_2/CO_2$_DMF-P-sl-6eq	$Cu_3(BTC)_2(NHEt_2)_{0.70}(EtOH)_{0.04}$	63.0	62.0
$CuCl_2/NHEt_2/CO_2$_EtOH-P-sl-6eq	$Cu_3(BTC)_2(NHEt_2)_{0.32}(EtOH)_{0.07}$	65.6	62.4

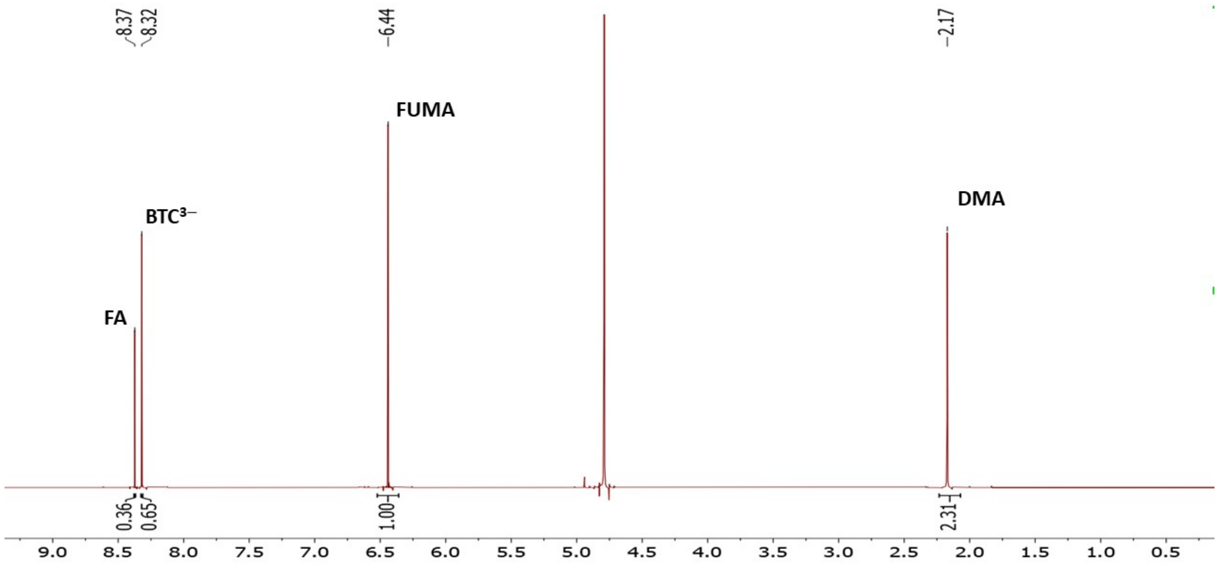

Figure S22: ^1H NMR spectrum of **CuOAc_DMF-P-T140-s** after digestion, using fumaric acid as internal standard. FA = formic acid; BTC^{3-} = 1,3,5-benzetricarboxylate anion; FUMA = fumaric acid; DMA = dimethylamine.

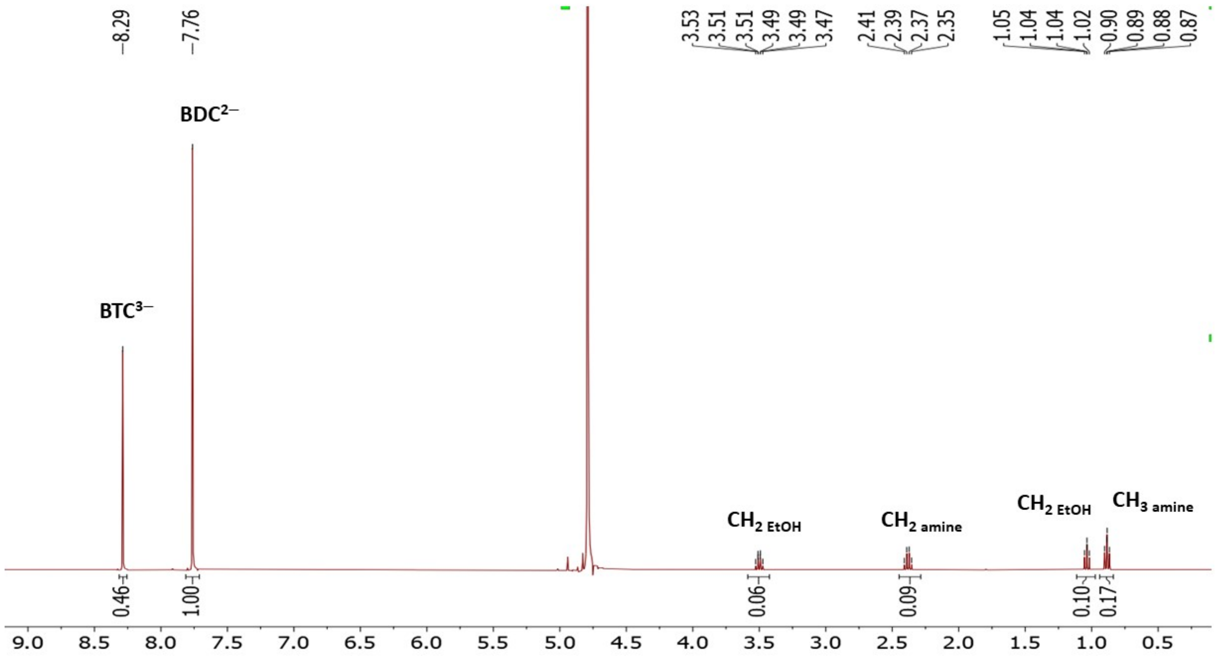

Figure S23: ^{1}H NMR spectrum of **CuCBM_DMF-P-sl** after digestion, using fumaric acid as internal standard. BTC^{3-} = 1,3,5-benzetricarboxylate anion; BDC^{2-} = 1,4-benzedicarboxylate anion.

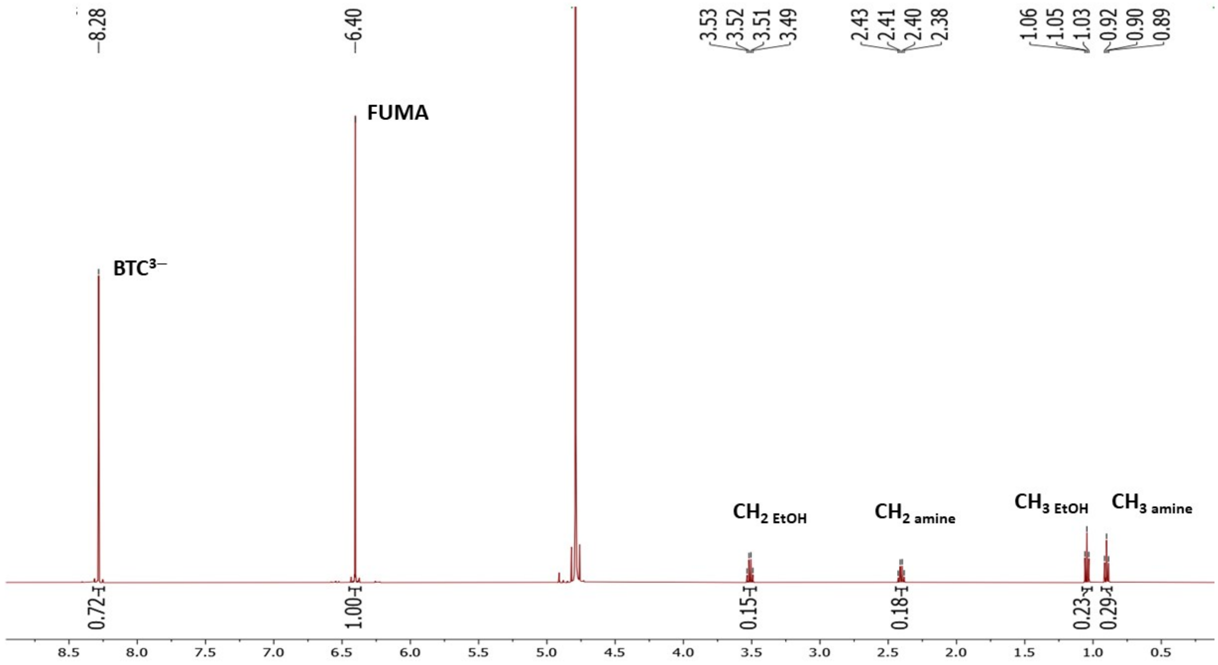

Figure S24: ^{1}H NMR spectrum of **CuCBM_EtOH-P-sl** after digestion, using fumaric acid as internal standard. BTC^{3-} = 1,3,5-benzetricarboxylate anion; FUMA = fumaric acid.

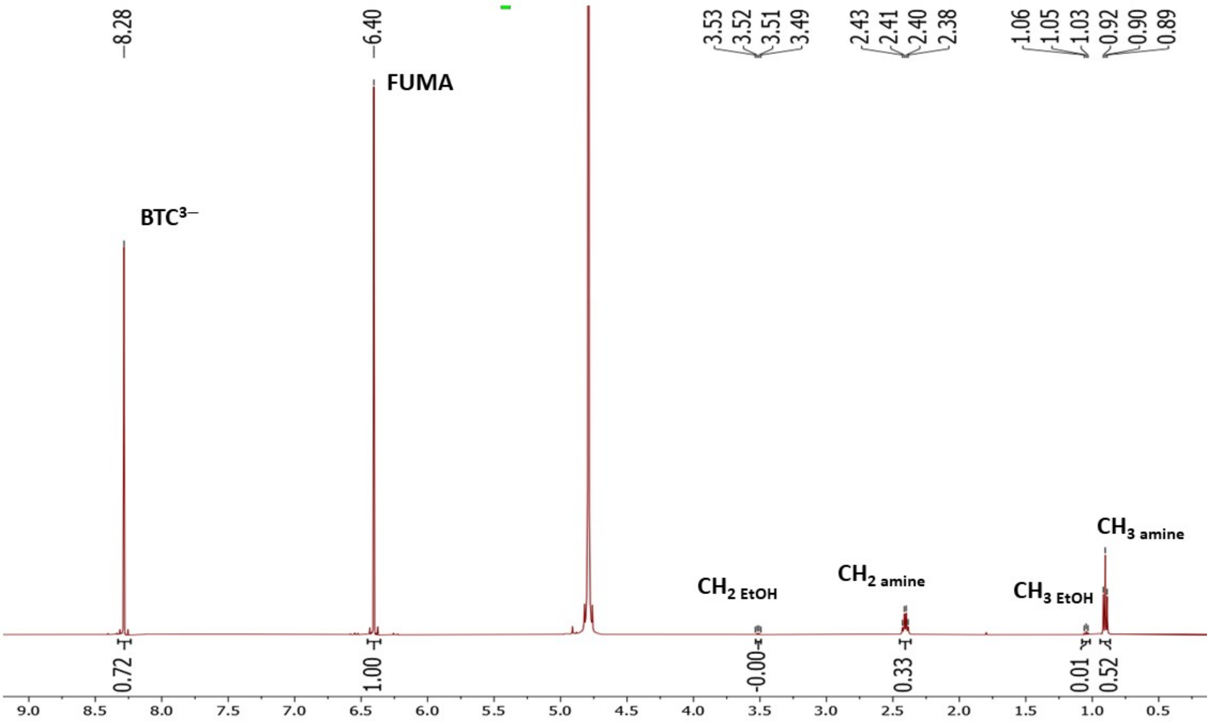

Figure S25: ^{1}H NMR spectrum of **$CuCl_2/NHEt_2/CO_2$_DMF-P-sl-6eq** after digestion, using fumaric acid as internal standard. BTC^{3-} = 1,3,5-benzetricarboxylate anion; FUMA = fumaric acid.

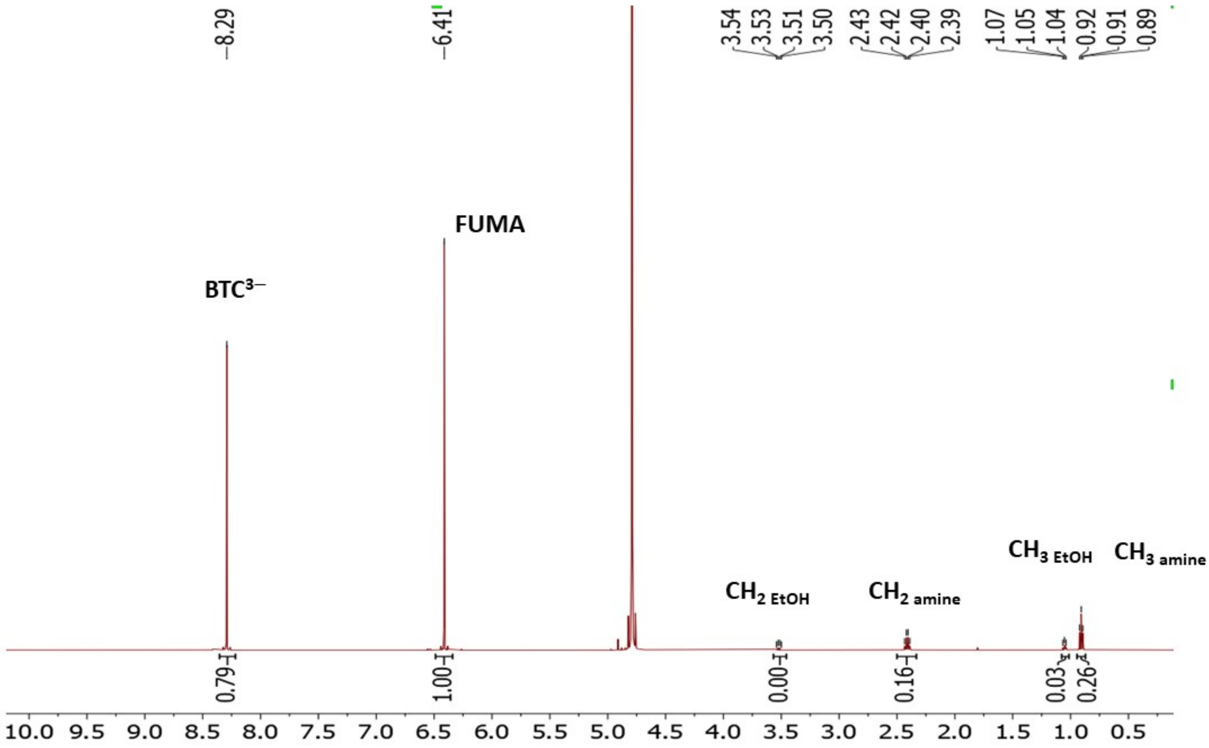

Figure S26: ^{1}H NMR spectrum of **$CuCl_2/NHEt_2/CO_2$_EtOH-P-sl-6eq** after digestion, using fumaric acid as internal standard. BTC^{3-} = 1,3,5-benzetricarboxylate anion; FUMA = fumaric acid.

Elemental Analysis

Sample preparation

About 2 mg of solid was introduced into a tin boat for elemental analysis and kept at 120 °C for two hours. Afterwards, the boat was closed while still hot and weighed to determine the mass of the desolvated solid to analyse.

Table S8: Calculated and experimental elemental analysis. Calculated percentages are based on the hypothetical formula based on ^{1}H-NMR spectra.

Sample	%C exp	%H exp	%N exp	Hypothetical Formula	%C calc	%H calc	%N calc
CuOAc_DMF-P-T140-s	37.17	3.99	5.13	$Cu_3(BTC)_2(DMF)_{3.30}$	39.50	3.42	5.40
CuCBM_DMF-P-sl	40.34	3.02	3.28	$Cu_3(BTC)_2(NHEt_2)_{0.96}(EtOH)_{0.85}$	39.58	3.06	1.88
CuCBM_EtOH-P-sl	36.61	2.00	1.04	$Cu_3(BTC)_2(NHEt_2)_{0.40}(EtOH)_{0.60}$	37.75	2.13	0.85
$CuCl_2$/$NHEt_2$/CO_2_DMF-P-sl-6eq	38.03	2.47	1.84	$Cu_3(BTC)_2(NHEt_2)_{0.70}(EtOH)_{0.04}$	38.12	2.13	1.49
$CuCl_2$/$NHEt_2$/CO_2_EtOH-P-sl-6eq	35.67	1.92	0.90	$Cu_3(BTC)_2(NHEt_2)_{0.32}(EtOH)_{0.07}$	36.93	1.59	0.71

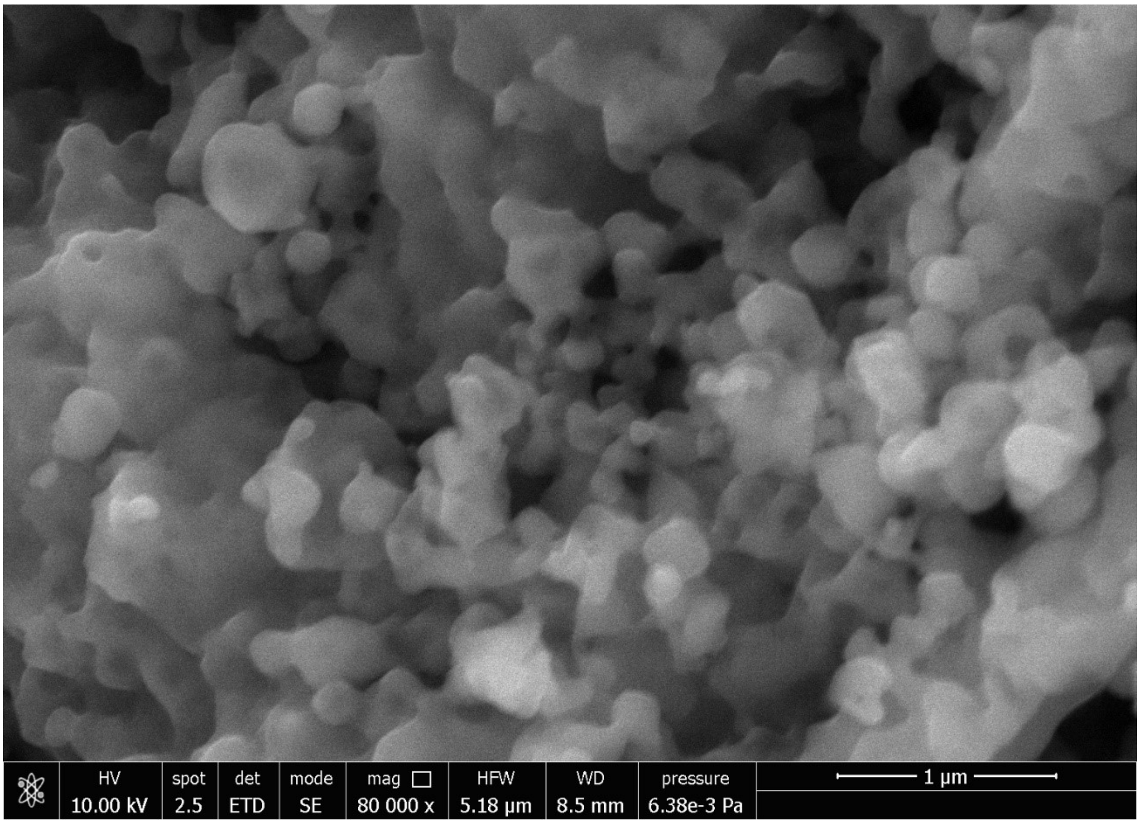

Figure S27: SEM image of **CuCBM_DMF-P-sl**.

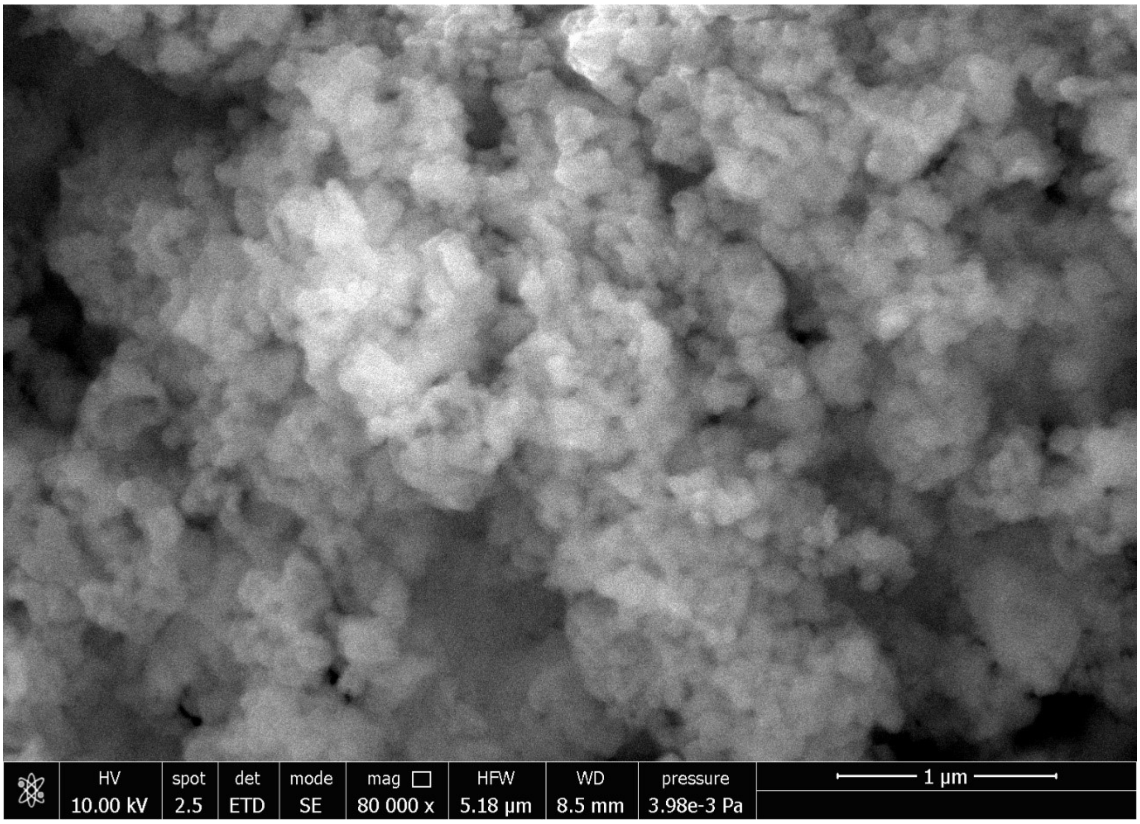

Figure S28: SEM image of **CuCBM_EtOH-P-sl**.

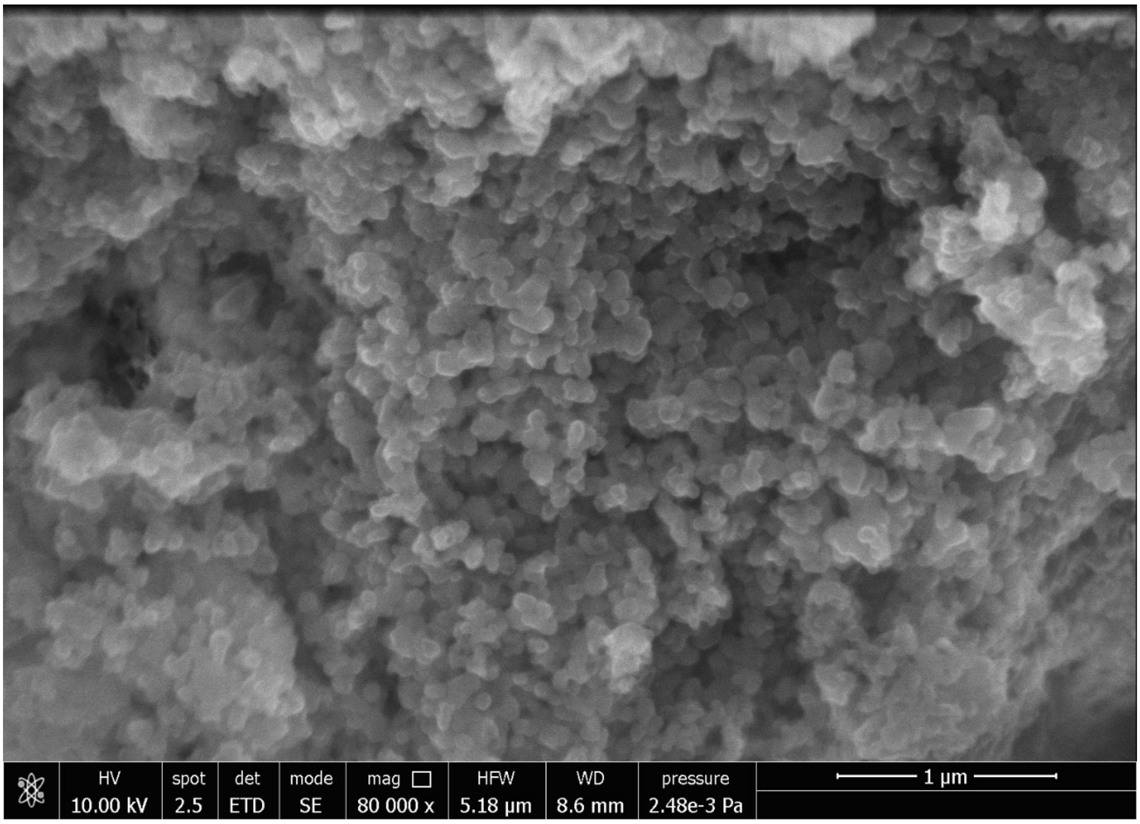

Figure S29: SEM image of **CuOAc_DMF-P-T140-s**.

Figure S30: SEM image of **$CuCl_2$/$NHEt_2$/CO_2_EtOH-P-sl-6eq**.

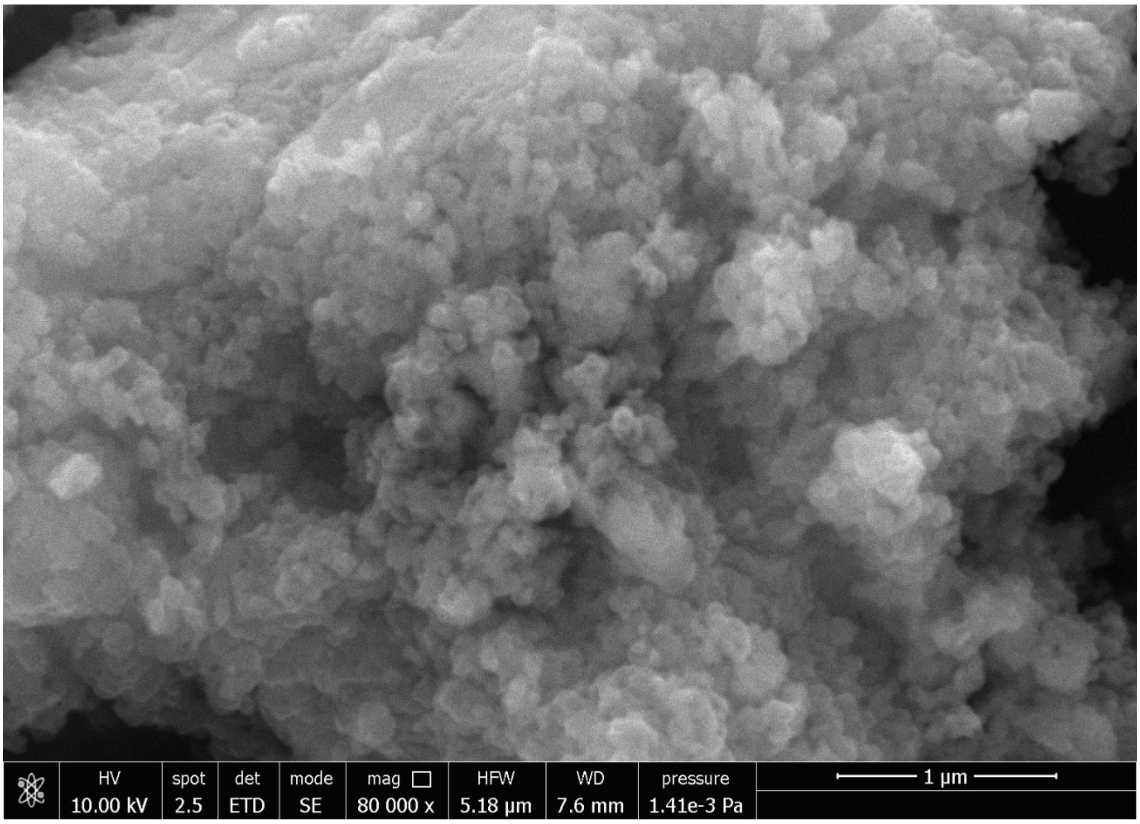

Figure S31: SEM image of **CuCl$_2$/NHEt$_2$/CO$_2$_DMF-P-sl-6eq**.

Table S9: N$_2$ sorption results for selected HKUST-1 samples.

Entry	**Sample name**	**Surface Area (m^2 g^{-1})**
1	**CuOAc_DMF-P-T140-s**	933
2	**CuCBM_DMF-P-sl**	543
3	**CuCBM_EtOH-P-sl**	1010
4	**CuCl$_2$/NHEt$_2$/CO$_2$_DMF-P-sl-6eq**	745
5	**CuCl$_2$/NHEt$_2$/CO$_2$_EtOH-P-sl-6eq**	1012

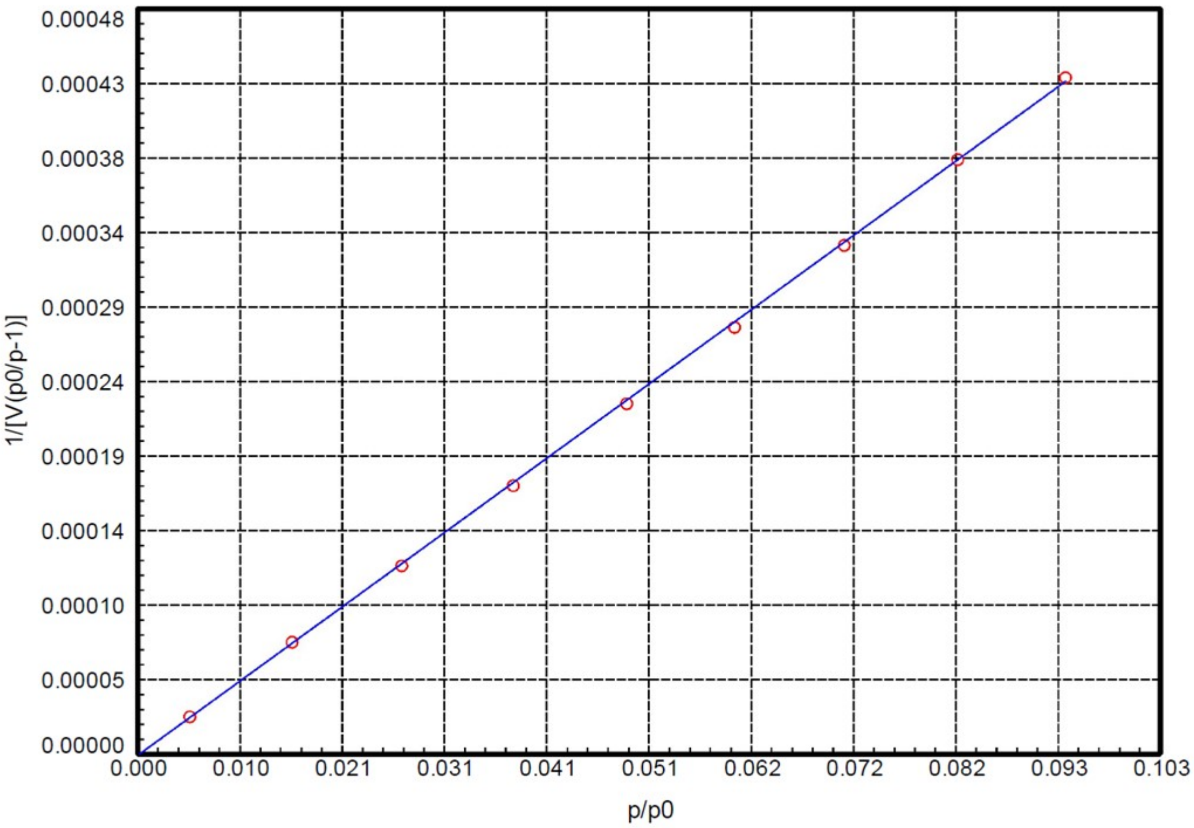

Figure S32: BET plot of **CuOAc_DMF-P-T140-s**.

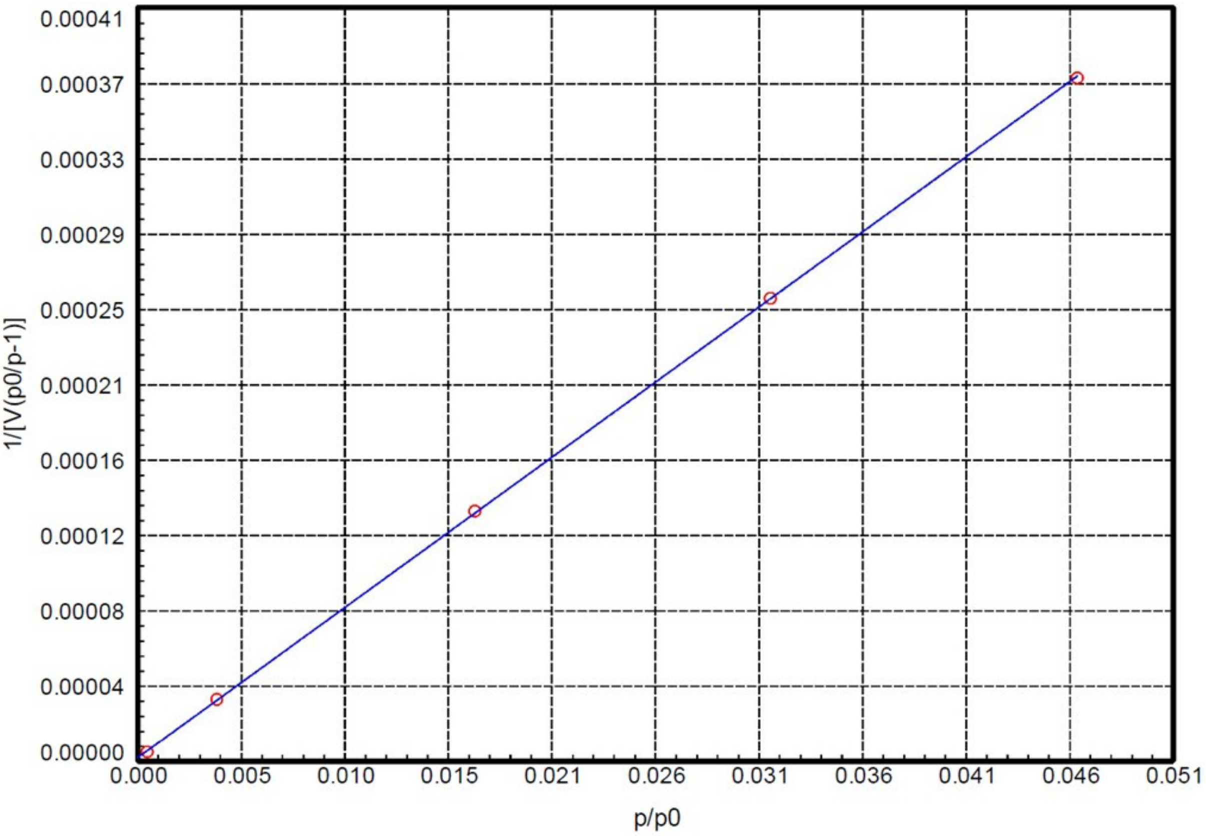

Figure S33: BET plot of **CuCBM_DMF-P-sl**.

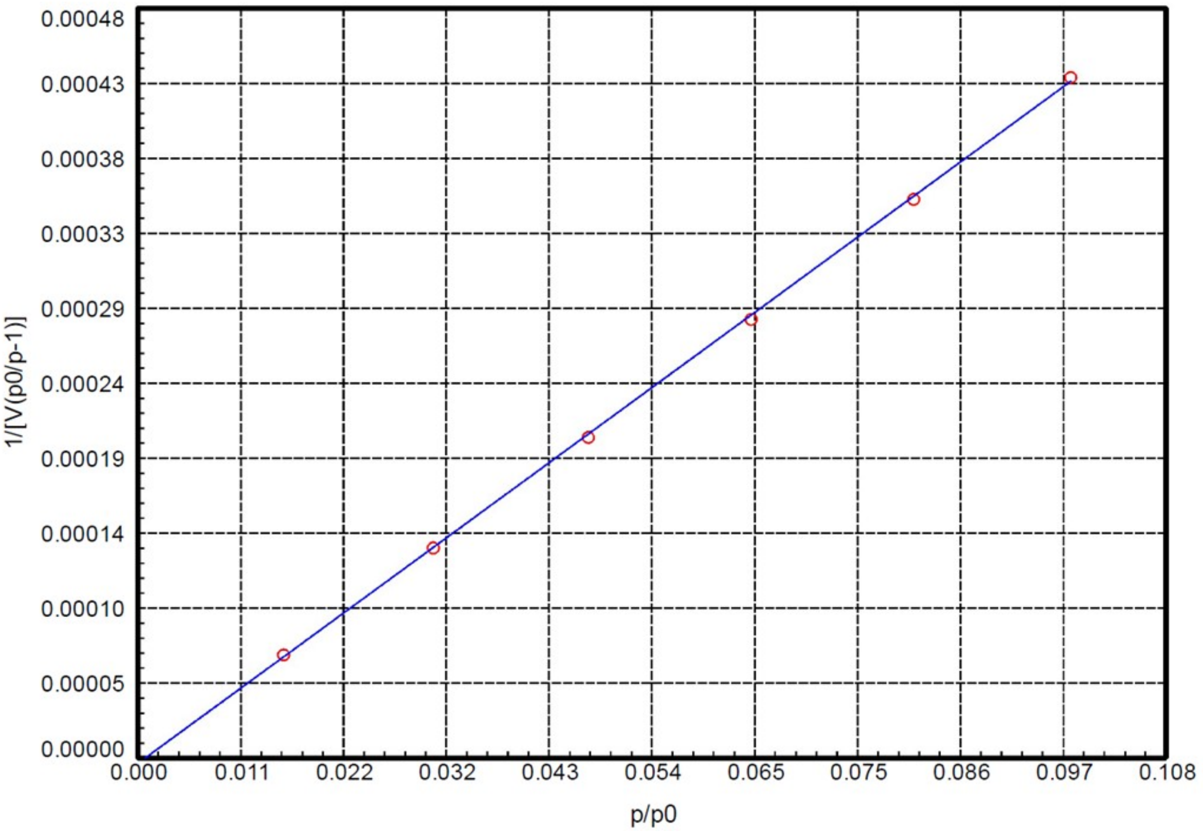

Figure S34: BET plot of **CuCBM_EtOH-P-sl**.

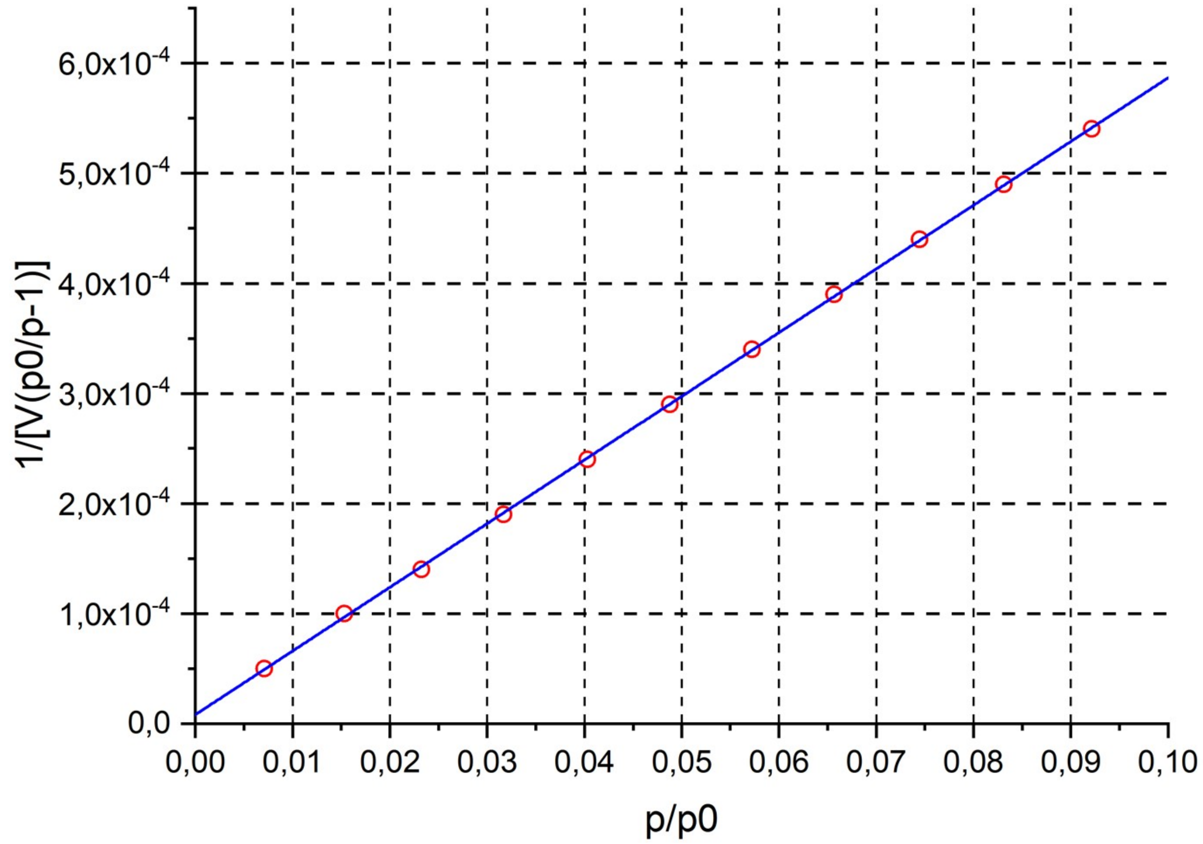

Figure S35: BET plot of **$CuCl_2$/$NHEt_2$/CO_2_DMF-P-sl-6eq**.

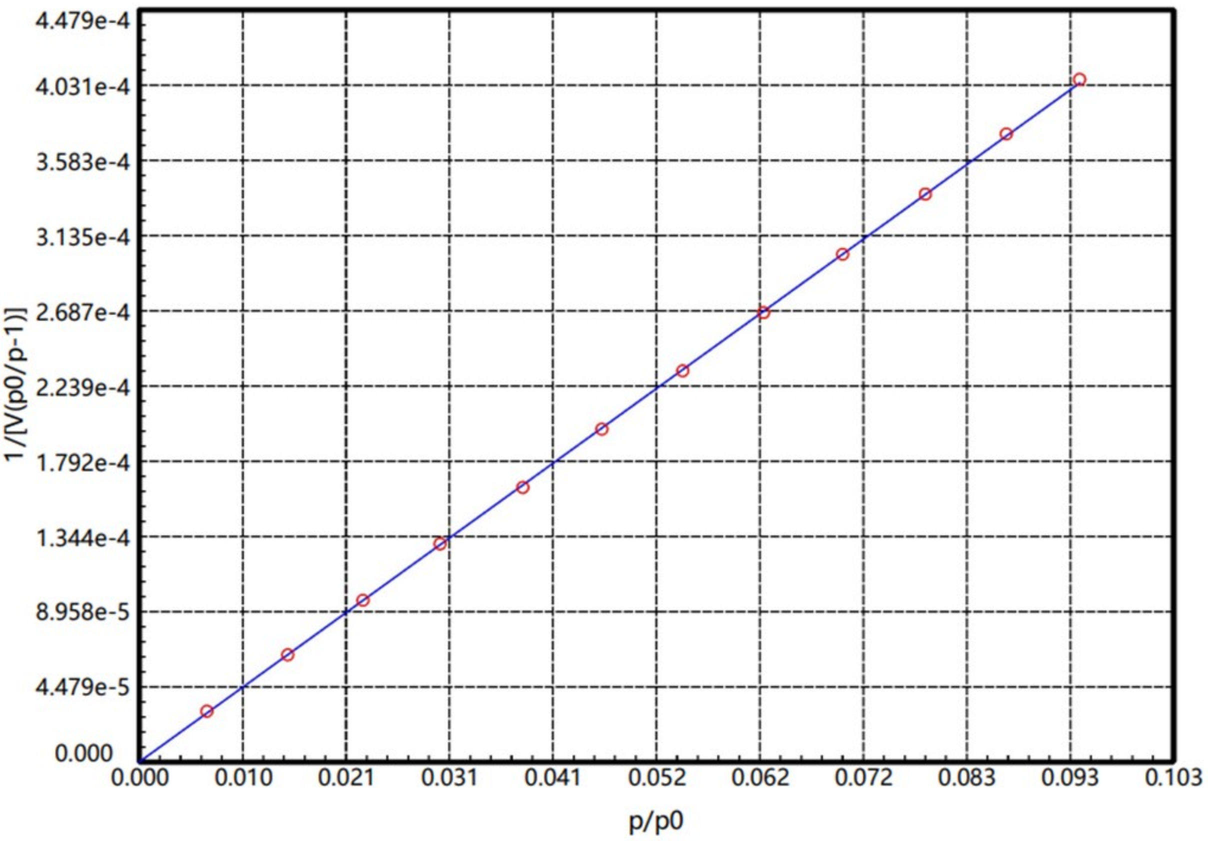

Figure S36: BET plot of **$CuCl_2$/$NHEt_2$/CO_2_EtOH-P-sl-6eq**.

Table S10: Comparison of the room temperature synthesis of HKUST-1 starting from **CuCBM** with room temperature methods starting from other metal precursors reported in the literature.

Metal precursor	**Solvent**	**Linker/metal ratio**	**Reaction time (h)**	**Yield (%)**	**BET Area ($m^2\ g^{-1}$)**	**Notes**	**Ref.**
CuCBM	EtOH	1:1	24	98[a]	1010	Linker solution added dropwise (2 mL h^{-1})	This work
$Cu(NO_3)_2{\cdot}3H_2O$	$EtOH/H_2O$	1:1	0	n.a.	940	Addition of diethylamine (amine/linker ratio = 3:1)	1
$Cu(NO_3)_2{\cdot}3H_2O$	$MeOH/H_2O$	1:1.8	30	96	1037	Addition of *N*,*N*,*N*,*N*-tetramethyl-1,6-hexanediamine (amine/linker ratio = 2.7:1)	2
$Cu(OAc)_2{\cdot}H_2O$	H_2O	2:1	24	n.a.	471	Cu solution added dropwise (25 mL h^{-1})	3
$CuCl_2$	H_2O/ionic liquid	1:1.5	0.5	96	1484	Ionic liquid is *N*,*N*,*N*,*N′*,*N′*,*N′*-hexakis(2-hydroxyethyl)ethane-1,2-diaminium bromide	4
$Cu(NO_3)_2{\cdot}3H_2O$	$MeOH/H_2O$	1:1.8	24	n.a.	989	Addition of 2-dimethylaminoethylamine (amine/Cu ratio = 2.7:1)	5
$Cu(NO_3)_2{\cdot}2.5H_2O$	H_2O	1:1.5	0	50	1372	pH = 3.3	6
$Cu(OAc)_2{\cdot}H_2O$	H_2O	2:1	1	97	1376	-	7

[a]Calculated based on the proposed formula in Table S8.

Table S11: Syntheses conducted in DMF without modulator. The precursor is: **ZrCBM** = Zr(IV) *N,N*-diethylcarbamate; **ZrCl$_4$** = Zirconium(IV) chloride. The linker is **P** = H$_2$BDC; **D^{I}**= HBDC^{-} and **D^{II}**=BDC^{2-}. FWHM (Full width at half maximum) was evaluated for the 111 reflection located at 7.4 °2θ.

Entry	Sample name	NHEt$_2$	T (°C)	Yield (mg)	FWHM (°)
1	**ZrCl$_4$_DMF-P-T120**	/	120	134	0.20
2	**ZrCBM_DMF-P-T120**	/	120	80	---[a]
3	**ZrCBM_DMF-P**	/	25	26	---[a]
4	**ZrCBM_DMF-D^{I}-T120**	1 eq	120	76	---[a]
5	**ZrCBM_DMF-D^{II}-T120**	2 eq	120	92	---[a]
6	**ZrCBM_EtOH-D^{II}-T55**	2 eq	55	27	---[a]
7	**ZrCl$_4$_EtOH-D^{II}-T55**	2 eq	55	55	---[a]
8	**ZrCBM_MeOH-D^{II}-T55**	2 eq	55	68	---[a]
9	**ZrCl$_4$_MeOH-D^{II}-T55**	2 eq	55	14	---[a]

[a]Amorphous product.

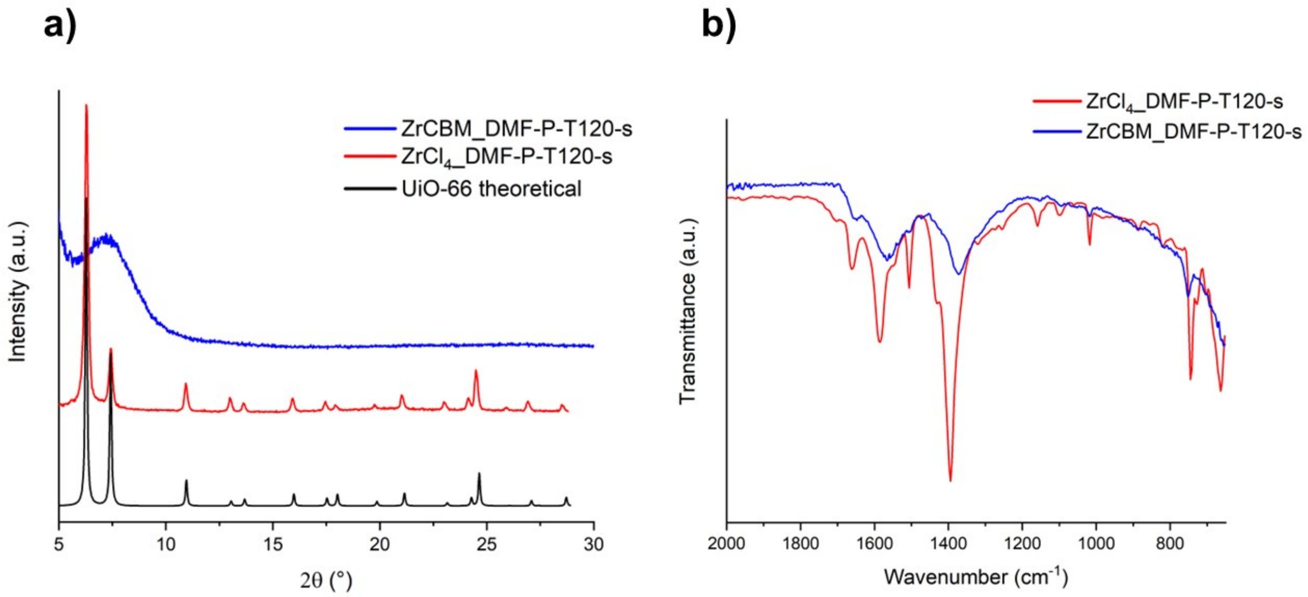

Figure S37: a) PXRD patterns of **ZrCBM_DMF-P-T120-s** (blue line) and **ZrCl$_4$_DMF-P-T120-s** (red line) compared with UiO-66 theoretical pattern (black line). b) IR spectra of **ZrCBM_DMF-P-T120-s** (blue line) and **ZrCl$_4$_DMF-P-T120-s** (red line).

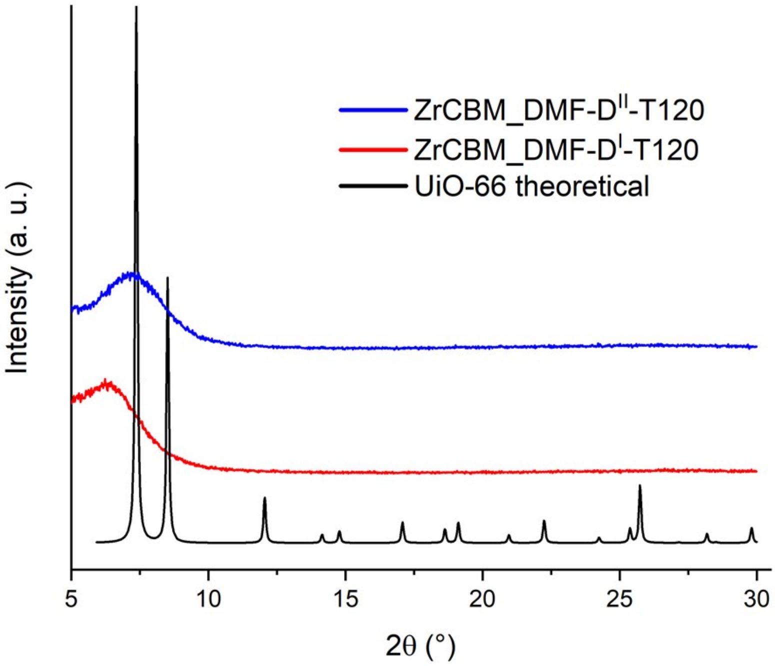

Figure S38: PXRD patterns of **ZrCBM_DMF-D^{II}-s** (blue line), **ZrCBM_DMF-D^{I}-s** (red line) compared with the theoretical one of UiO-66 (black line).

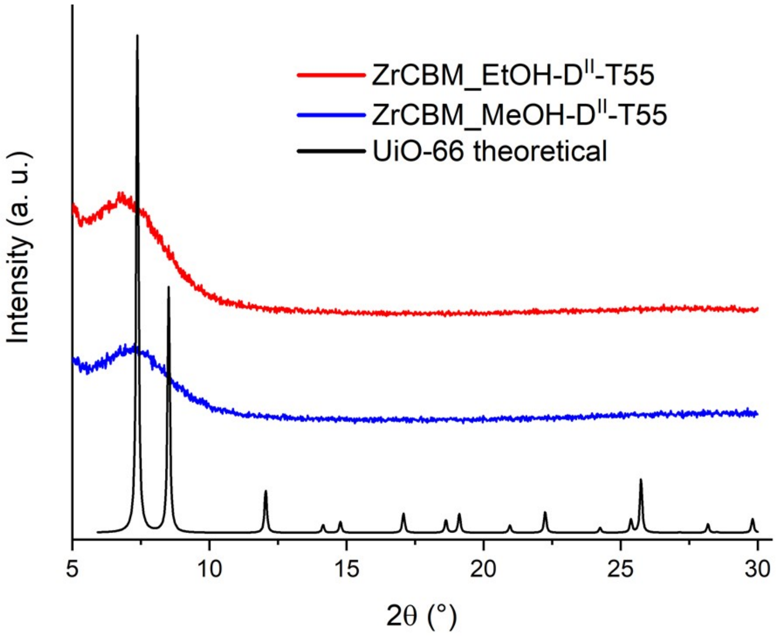

Figure S39: PXRD patterns of **ZrCBM_EtOH-D^{II}-T55** (red line) and **ZrCBM_MeOH-D^{II}-T55** (blue line) compared with the theoretical pattern of UiO-66 (black line).

Table S12: Syntheses conducted in DMF with formic acid as modulator. The precursors are: **ZrCBM** = Zr(IV) *N,N*-diethylcarbamate, **$ZrCl_4$** = Zirconium(IV) chloride The linker is **P** = H_2BDC. The symbol **@** was used when $NHEt_2$ was added into the system after the linker. The m(equivalents of modulator) is the molar ratio between FA and Zr. FWHM (Full width at half maximum) was evaluated for the 111 reflection located at 7.4 °2θ.

Entry	Sample name	$NHEt_2$ (eq)	Mod (eq)	Yield (mg)	FWHM (°)
1	**ZrCBM_DMF-P-T120-m100**	/	100	75	0.32
2	**ZrCBM_DMF-P-m100**	/	100	86	0.38
3	**$ZrCl_4$_DMF-P-T120-m100@**	4	100	54	0.23
4	**$ZrCl_4$_DMF-P-m100@**	4	100	70	0.84
5	**ZrCBM_DMF-P-t1-m100**	/	100	58	0.38
6	**ZrCBM_DMF-P-t3-m100**	/	100	71	0.39
7	**ZrCBM_DMF-P-m50**	/	50	86	0.94
8	**ZrCBM_DMF-P-m150**	/	150	95	0.22

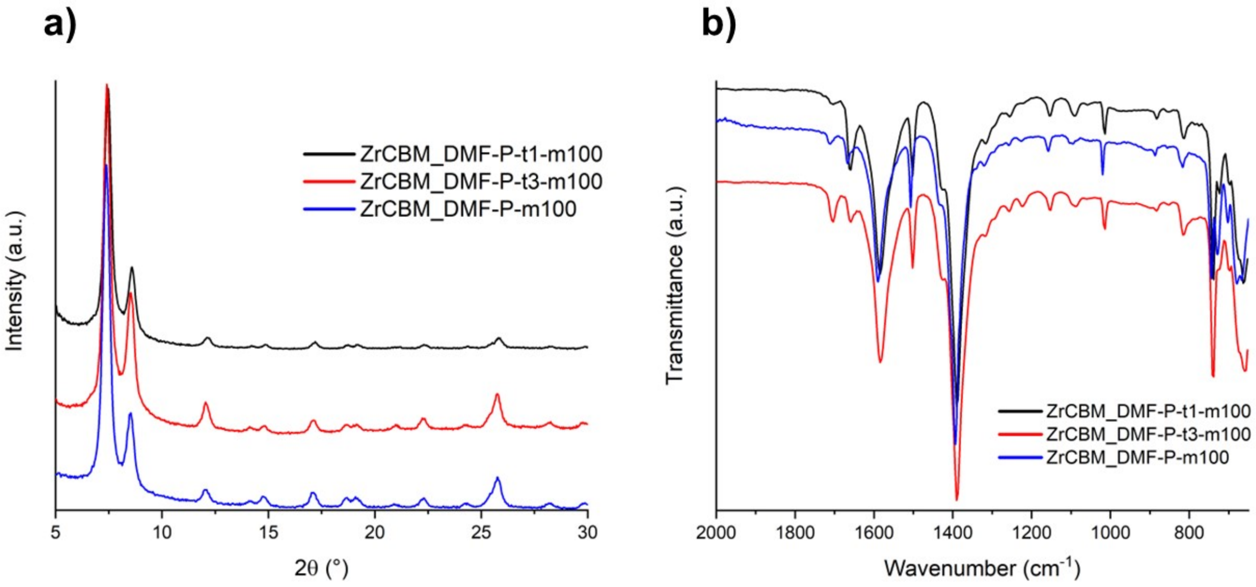

Figure S40: PXRD patterns (a) and IR spectra (b) of **ZrCBM_DMF-P-t1-m100** (black line), **ZrCBM_DMF-P-t3-m100** (red line), **ZrCBM_DMF-P-m100** (blue line).

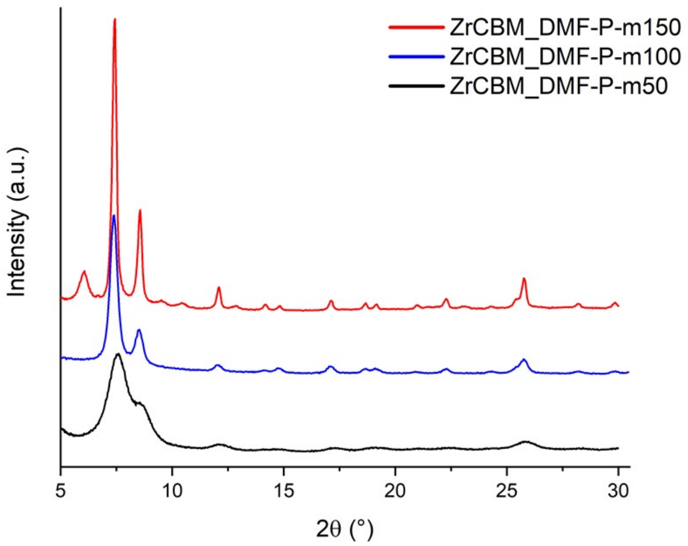

Figure S41: PXRD patterns of **ZrCBM_DMF-P-m150** (red line), **ZrCBM_DMF-P-m100** (blue line) and **ZrCBM_DMF-P-m150** (black line).

Table S13: Theoretical and experimental percentage of BDC^{2-} ligand for UiO-66 samples calculated by ^{1}H-NMR.

Sample	Hypothetical Formula	BDC^{2-} theo (%)	BDC^{2-} exp (%)
ZrCBM_DMF-P-m100	$Zr_6O_4(OH)_4(BDC)_{4.25}(FA)_{3.50}$	45.8	51.6
ZrCBM_DMF-P-T120-m100	$Zr_6O_4(OH)_4(BDC)_{5.02}(FA)_{1.96}$	51.8	53.3
ZrCl$_4$_DMF-P-m100$^@$	$Zr_6O_4(OH)_4(BDC)_{3.91}(FA)_{4.18}(DEA)_{0.28}$	41.9	30.3
ZrCl$_4$_DMF-P-T120-m100$^@$	$Zr_6O_4(OH)_4(BDC)_{4.80}(FA)_{2.40}$	50.0	52.0

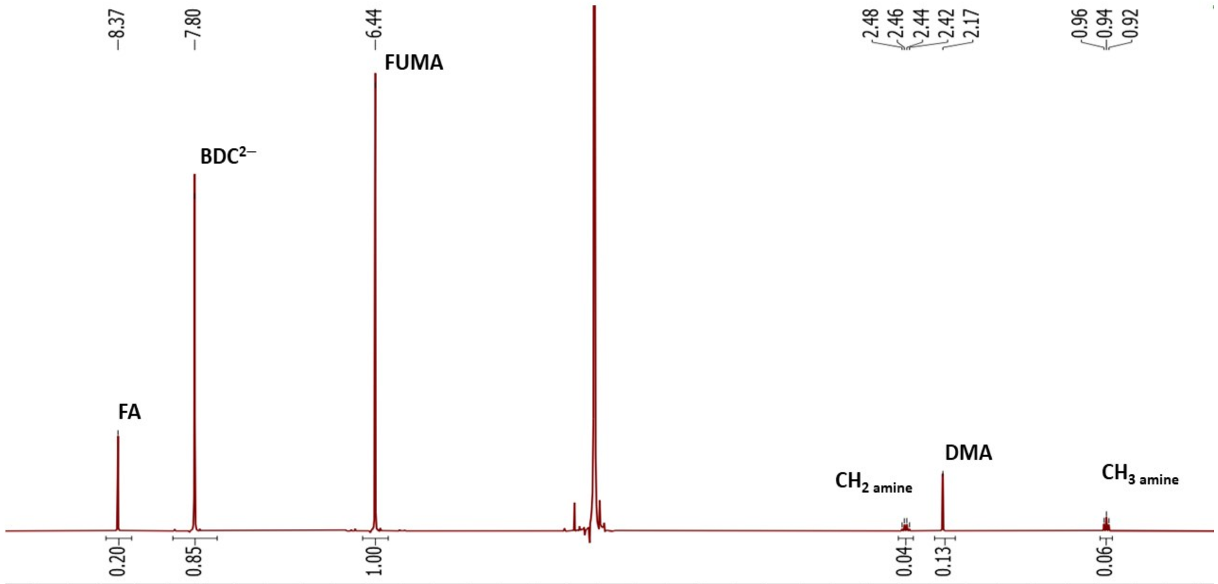

Figure S42: ^{1}H NMR spectrum of **ZrCBM_DMF-P-m100** after digestion, using fumaric acid as internal standard. FA = formic acid; BDC^{2-} = 1,4-benzedicarboxylate anion; FUMA = fumaric acid; DMA = dimethylamine.

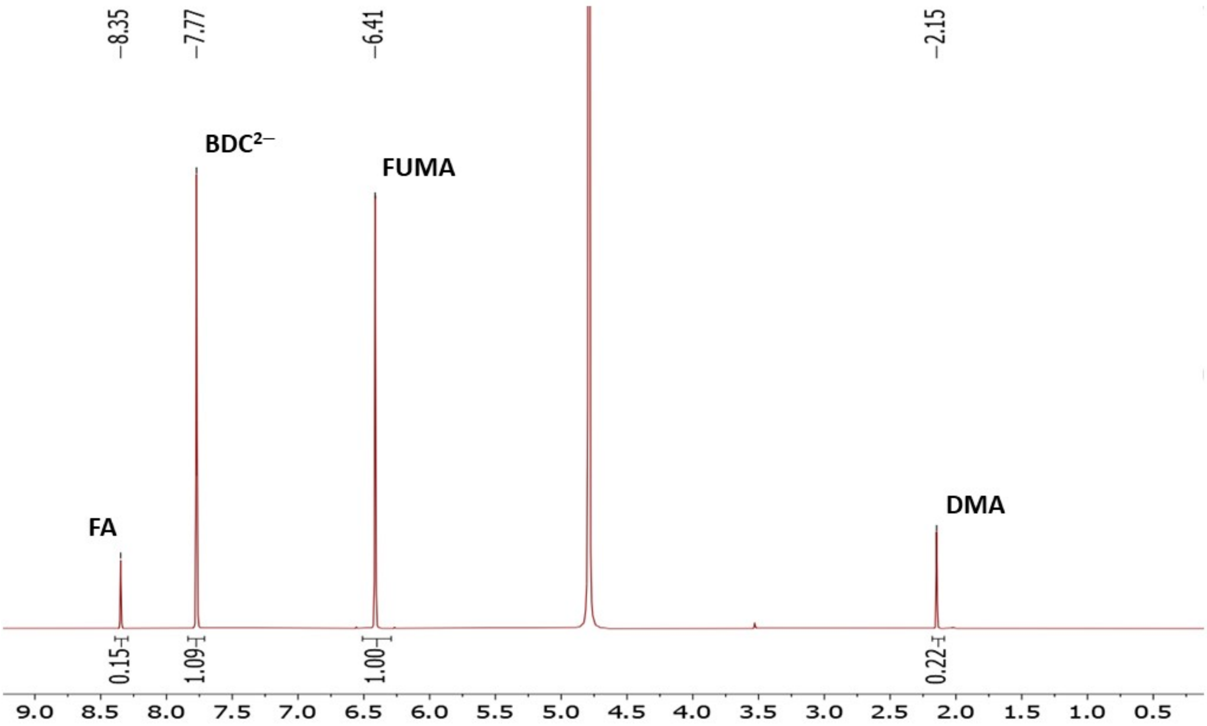

Figure S43: ^{1}H NMR spectrum of **ZrCBM_DMF-P-T120-m100** after digestion, using fumaric acid as internal standard. FA = formic acid; BDC^{2-} = 1,4-benzedicarboxylate anion; FUMA = fumaric acid; DMA = dimethylamine.

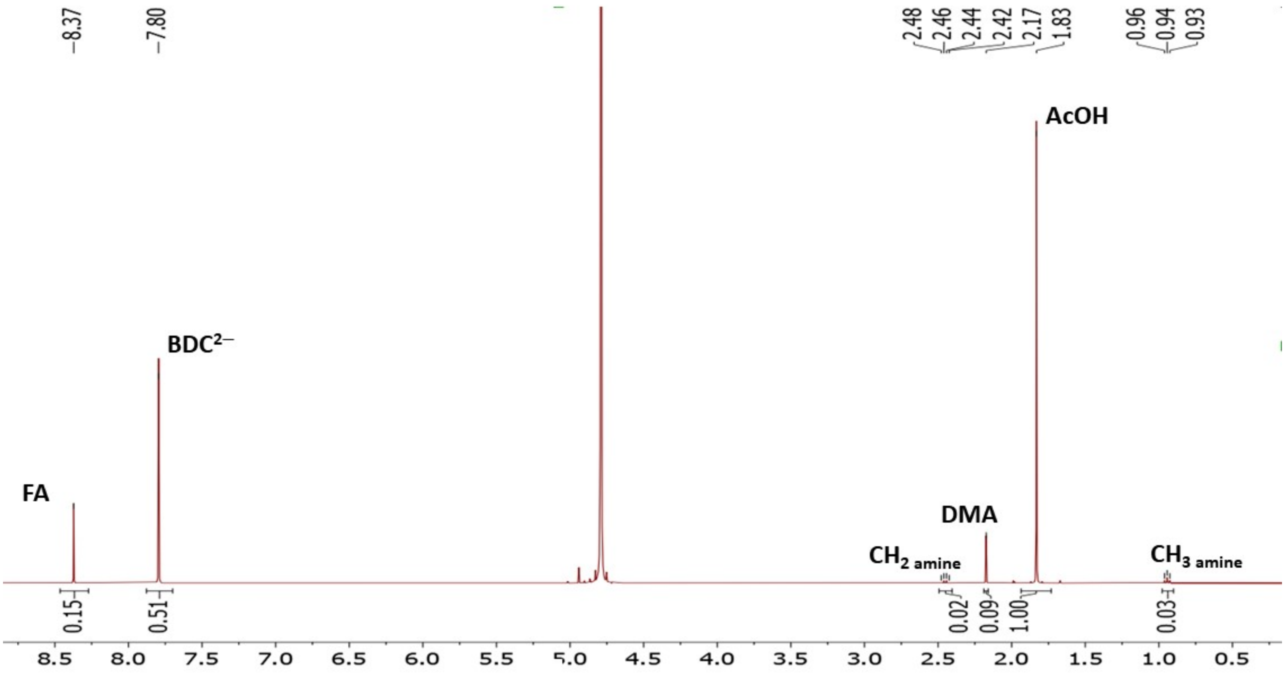

Figure S44: ^{1}H NMR spectrum of **ZrCl4_DMF-m100$^{@}$** after digestion, using acetic acid as internal standard. FA = formic acid; BDC^{2-} = 1,4-benzedicarboxylate anion; DMA = dimethylamine; AcOH = acetic acid.

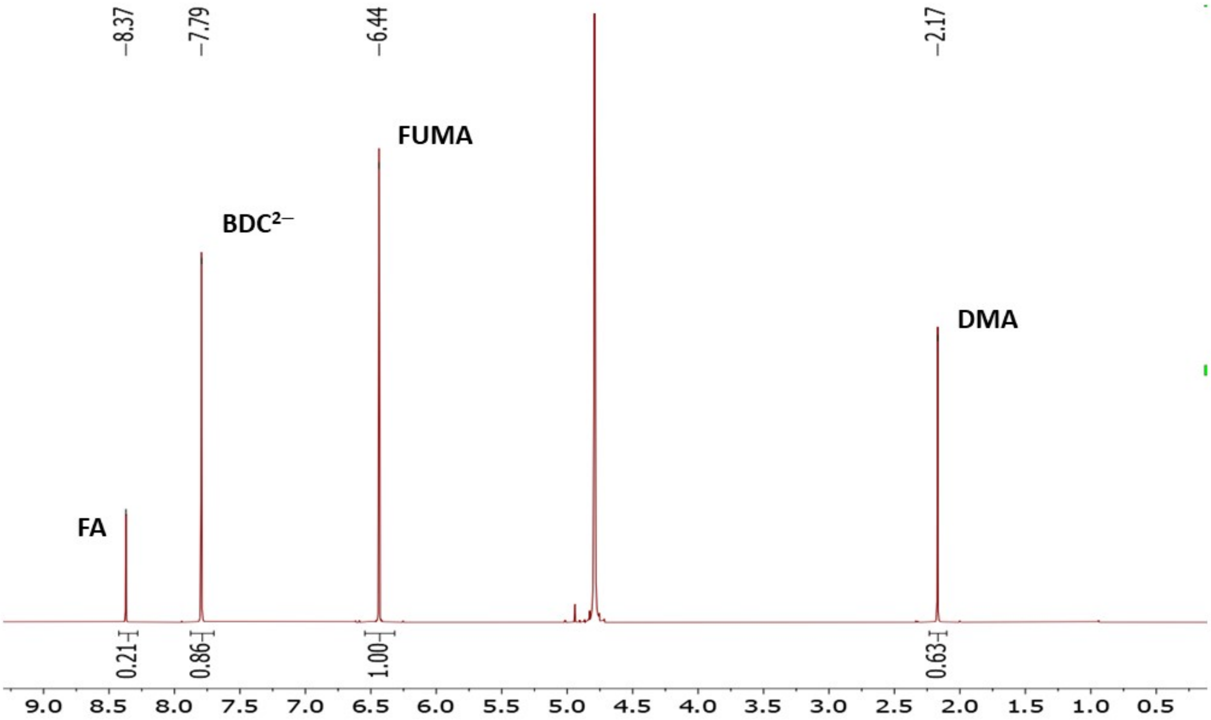

Figure S45: ^{1}H NMR spectrum of **ZrCl4_DMF-T120-m100@** after digestion, using fumaric acid as internal standard. FA = formic acid; BDC^{2-} = 1,4-benzedicarboxylate anion; FUMA = fumaric acid; DMA = dimethylamine.

Table S14: N_2 sorption results of selected samples.

Entry	Sample name	Surface Area [m^2/g]
1	**ZrCBM_DMF-P-T120-m100**	941
2	**ZrCBM_DMF-P-m100**	1138
3	**ZrCl$_4$_DMF-T120-m100$^@$**	1684
4	**ZrCl$_4$_DMF-P-m100$^@$**	1100

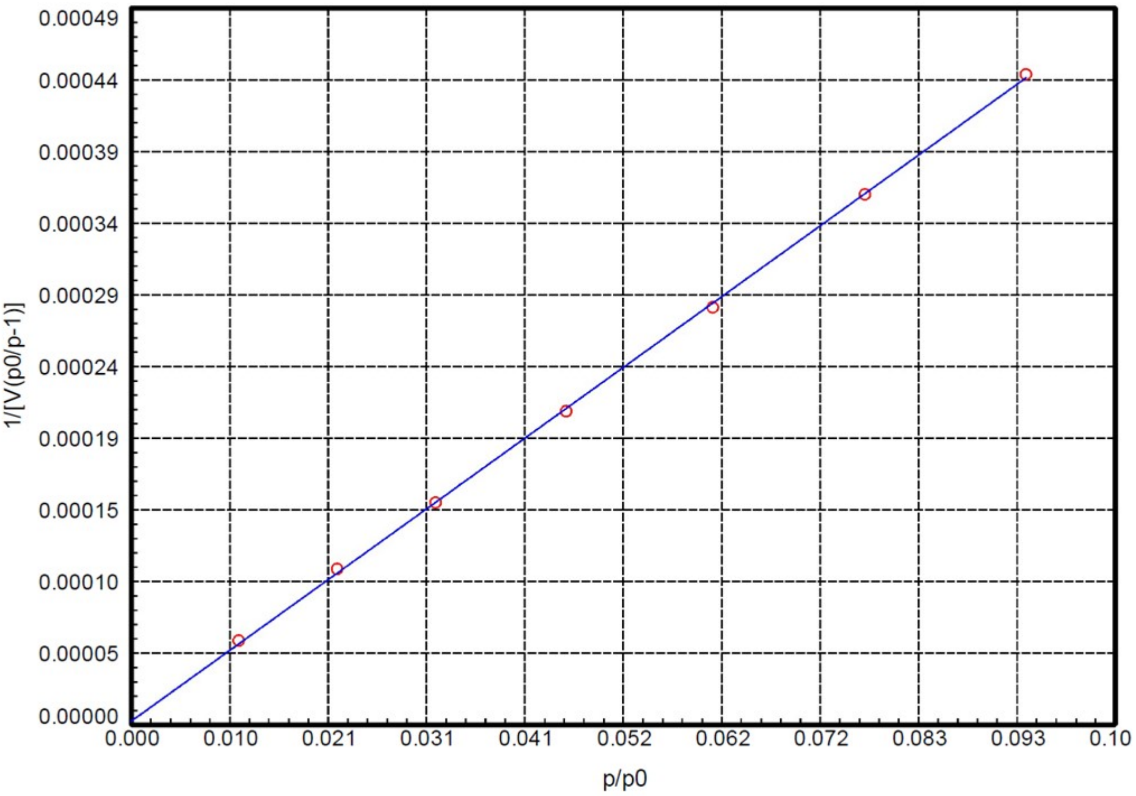

Figure S46: BET plot of **ZrCBM_DMF-P-T120-m100**.

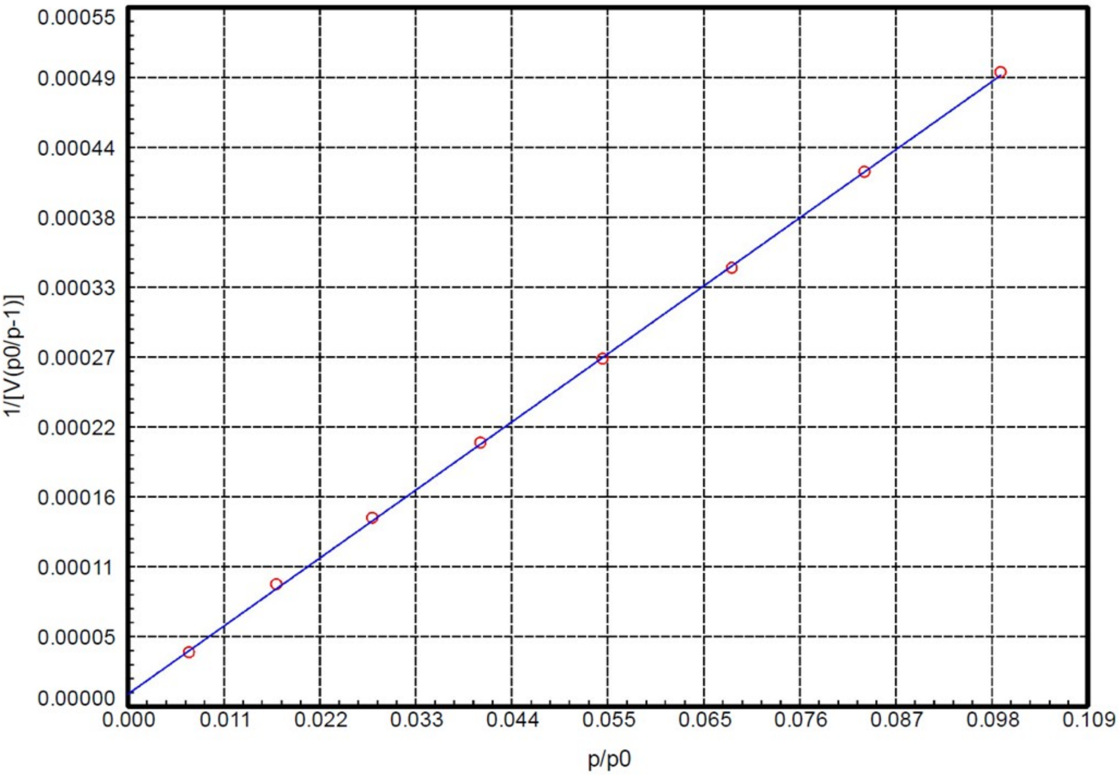

Figure S47: BET plot of **ZrCBM_DMF-P-m100**.

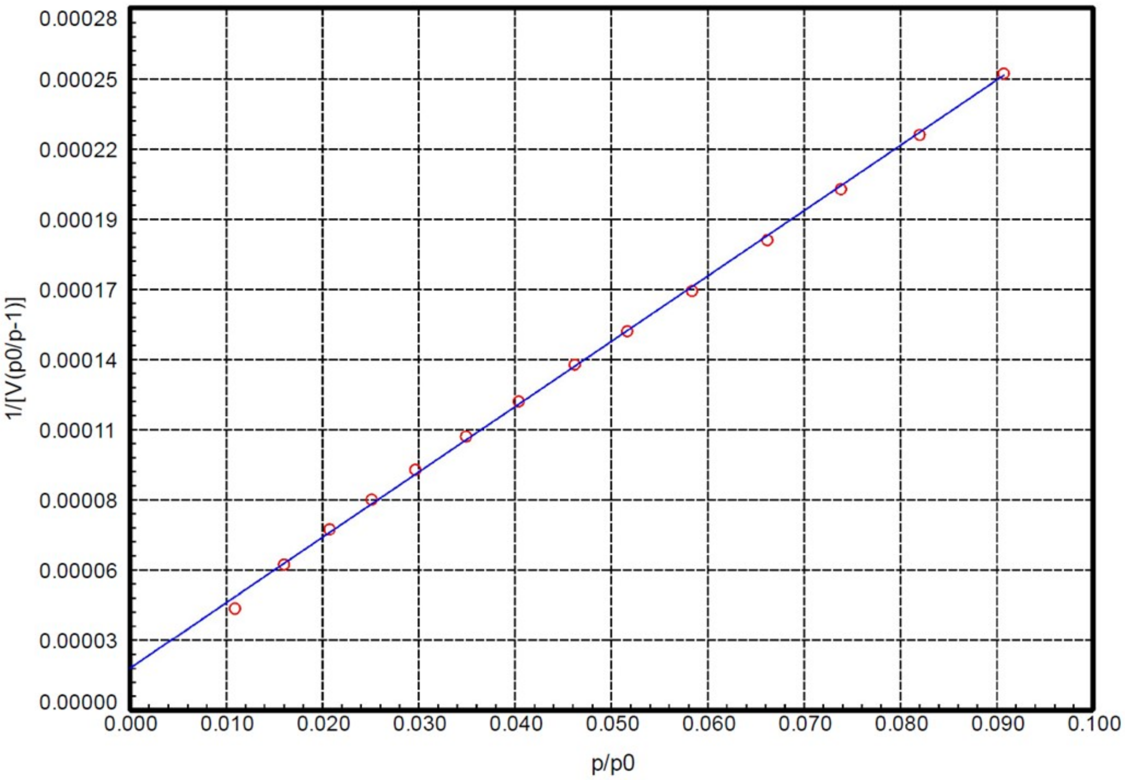

Figure S48: BET plot of **$ZrCl_4$_DMF-T120-m100$^{@}$**.

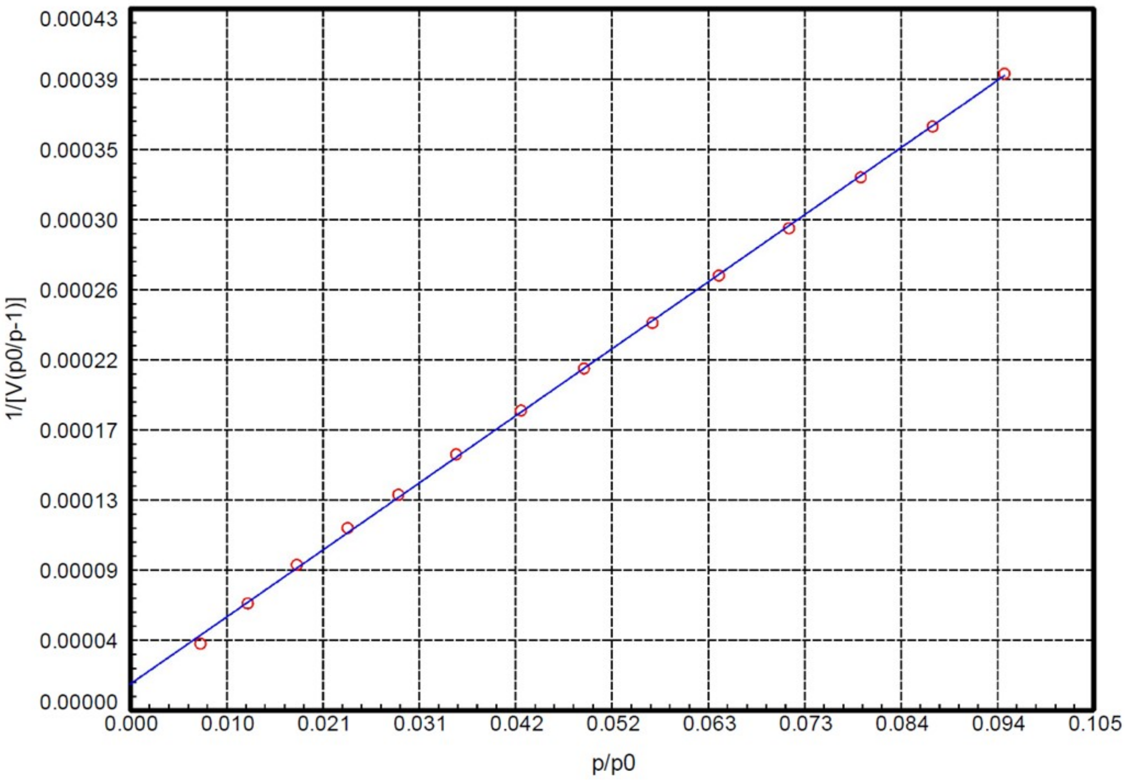

Figure S49: BET plot of **$ZrCl_4$_DMF-P-m100$^{@}$**.

Table S15: Comparison of the room temperature synthesis of UiO-66 starting from **ZrCBM** with room temperature methods starting from other metal precursors reported in the literature.

Metal precursor	Solvent	Linker/metal ratio	Reaction time (h)	Yield (%)	BET Area (m^2 g^{-1})	Notes	Ref.
ZrCBM	DMF	1:1	24	77[a]	1138	Addition of formic acid (formic acid/Zr ratio = 100:1)	This work
Zr(O*n*-Pr)$_4$	DMF/acetic acid	2.85:1	16	n.a.	1450	Acetic acid/Zr ratio = 443; reaction mixture is treated at 130 °C for 2 h prior to addition of the linker	8
$ZrOCl_2 \cdot 8H_2O$	H_2O/acetic acid	1:1	0	13	339	pH = 4.9	6

[a] Calculated based on the formula in Table S13.

References

(1) Majano, G.; Pérez-Ramírez, J. Room Temperature Synthesis and Size Control of HKUST-1. *HCA* **2012**, *95* (11), 2278–2286. https://doi.org/10.1002/hlca.201200466.

(2) Duan, C.; Yu, Y.; Li, F.; Wu, Y.; Xi, H. Ultrafast Room-Temperature Synthesis of Hierarchically Porous Metal–Organic Frameworks with High Space–Time Yields. *CrystEngComm* **2020**, *22* (15), 2675–2680. https://doi.org/10.1039/C9CE01676G.

(3) Siew, W. Y.; Abu Bakar, N. H. H.; Abu Bakar, M. The Influence of Green Synthesis on the Formation of Various Copper Benzene-1,3,5-Tricarboxylate Compounds. *Inorganica Chimica Acta* **2018**, *482*, 53–61. https://doi.org/10.1016/j.ica.2018.05.008.

(4) Fan, C.; Dong, H.; Liang, Y.; Yang, J.; Tang, G.; Zhang, W.; Cao, Y. Sustainable Synthesis of HKUST-1 and Its Composite by Biocompatible Ionic Liquid for Enhancing Visible-Light Photocatalytic Performance. *Journal of Cleaner Production* **2019**, *208*, 353–362. https://doi.org/10.1016/j.jclepro.2018.10.141.

(5) Duan, C.; Li, F.; Luo, S.; Xiao, J.; Li, L.; Xi, H. Facile Synthesis of Hierarchical Porous Metal-Organic Frameworks with Enhanced Catalytic Activity. *Chemical Engineering Journal* **2018**, *334*, 1477–1483. https://doi.org/10.1016/j.cej.2017.11.086.

(6) Huelsenbeck, L.; Luo, H.; Verma, P.; Dane, J.; Ho, R.; Beyer, E.; Hall, H.; Geise, G. M.; Giri, G. Generalized Approach for Rapid Aqueous MOF Synthesis by Controlling Solution pH. *Crystal Growth & Design* **2020**, *20* (10), 6787–6795. https://doi.org/10.1021/acs.cgd.0c00895.

(7) Huo, J.; Brightwell, M.; El Hankari, S.; Garai, A.; Bradshaw, D. A Versatile, Industrially Relevant, Aqueous Room Temperature Synthesis of HKUST-1 with High Space-Time Yield. *J. Mater. Chem. A* **2013**, *1* (48), 15220. https://doi.org/10.1039/c3ta14409g.

(8) DeStefano, M. R.; Islamoglu, T.; Garibay, S. J.; Hupp, J. T.; Farha, O. K. Room-Temperature Synthesis of UiO-66 and Thermal Modulation of Densities of Defect Sites. *Chem. Mater.* **2017**, *29* (3), 1357–1361. https://doi.org/10.1021/acs.chemmater.6b05115.